Colloquium: Star-branched polyelectrolytes: The physics of their conformations and interactions

Arben Jusufi*

Department of Chemical Engineering, Princeton University, Princeton, New Jersey 08540, USA

Christos N. Likos†

Institute of Theoretical Physics, Heinrich-Heine-Universität Düsseldorf, Universitätsstraße 1, D-40225 Düsseldorf, Germany

(Published 15 December 2009)

Recent progress in the field of a versatile and common system in soft matter physics, namely, star-shaped polyelectrolytes, is reviewed. These charged macromolecules combine in their properties aspects of polymer physics, colloidal science, and the rich physics of charged matter, rendering them into versatile building blocks for new materials as well as prototypes for studying the effects of softness in the behavior of colloidal suspensions. The approaches to the problem are manifold. Theoretical methods typically involve scaling theory, self-consistent field theory, and variational free-energy calculations, while computer simulations play an important role in enhancing our understanding of the physics involved. Experiments, based mostly on scattering, offer insights from a different point of view. Finally, the flexibility in the synthesis of novel types of macromolecules has added to the richness and the increased activity in the field in the last few years. This review puts emphasis on theory and simulation but takes into account the key experimental findings in critically discussing the merits and shortcomings of the former. The perspectives opened for the future, with emphasis on the possibilities to steer the behavior of novel materials, are also discussed.

DOI: 10.1103/RevModPhys.81.1753 PACS number(s): 82.35.Rs, 82.35.Gh, 82.39.Wj, 82.70.−y

CONTENTS

I. INTRODUCTION

Linear polyelectrolytes are polymer chains that carry ionizable groups along their backbones, which dissociate in aqueous solvents, leaving behind a charged polymer [a polyelectrolyte (PE)] and free counterions in solution. PEs are important macromolecules due to their rich physics and their relevance in applications. When f such PEs are anchored at one common end on a fixed center, star-branched PEs or, for brevity, polyelectrolyte stars (PE stars) are obtained. Star-shaped polymer aggregates in general constitute a particular class of macromolecules with high relevance in soft matter physics, chemistry, and materials science. Their common property is that they serve as hybrid systems between linear polymers and spherical soft colloids. Indeed, the presence of the penetrable polymer corona gives them properties that are unique since they are considerably more stiff than single chains but at the same time much softer than hard colloidal particles, such as the common (poly)-methyl-methacrylate hard spheres. The polymer corona endows star-shaped macromolecules with a potential energy barrier that acts as a mechanism against coagulation of the central colloids on which the chains are grafted. They also bear close resemblance to self-organized block-copolymer micelles and they can be considered as strongly curved polymer brushes. The local monomer profile within the corona of star-shaped polymers and their overall size, as well as their effective interactions and the ensuing correlations in concentrated solutions, depend on a number of parameters. For neutral polymers, the number of attached chains (functionality) f as well as the solvent quality are the key factors; for the case of self-organized starlike micelles the former can be externally tuned via solvent selectivity

*Present address: Institute for Computational Molecular Science, College of Science and Technology, Temple University, 1900 North Street, Philadelphia, PA 19122, USA. ajusufi@temple.edu

†Present address: Faculty of Physics, University of Vienna, Sensengasse 8/12, A-1090, Vienna, Austria. christos.likos@univie.ac.at

(Stellbrink *et al.*, 2004), whereas the latter is usually influenced by changing the temperature (Kapnistos *et al.*, 2000). For PE stars, the degree of charging α (fraction of monomers that carry charge), the salt concentration c_s, and the valency of counterions and coions, as well as the temperature and pH of the solution, are additional and relevant physical parameters that have an impact on all properties mentioned above. It follows that PE stars are therefore a physical system with rich physics and with correspondingly high relevance for the construction of novel materials, whose properties can be externally tuned. For the latter, application of external, electric fields are one more possibility since the charged macromolecules respond to them by conformational changes and transport.

Neutral star polymers, at least in athermal solvents, are nowadays well understood as a result of intensive research in the last three decades [see Grest *et al.* (1996) and Likos (2006) for reviews on the experimental and theoretical sides, respectively]. Relatively less is known about PE stars, although by now a significant number of complementary approaches from experiment, theory, and simulation have accumulated, so that a coherent picture has emerged. From the materials point of view, the most common polyelectrolytes employed in chemically synthesized PE stars are sodium-sulphonated polysterene (Heinrich *et al.*, 2001) and polyacrylic acid (Furukawa and Ishizu, 2005; Plamper *et al.*, 2005). Often, PE stars are obtained by self-association of micelle-forming block copolymers (Muller *et al.*, 2000; Korobko *et al.*, 2004, 2005). Their overall charge and the ensuing conformations can be influenced by changing the pH of the solution (Gorodyska *et al.*, 2003; Kiryi *et al.*, 2003).

Closely related to PE stars are spherical polyelectrolyte *brushes* (SPBs), for which the size of the central colloid on which the PEs are grafted is at least comparable if not larger than the brush height. Here recent advances in synthesis have led to the construction of SPBs by employing colloids on which stiff double-stranded DNA molecules (Kegler *et al.*, 2007, 2008) or semiflexible filamentous viruses (Huang *et al.*, 2008) are grafted. As the relative colloid-to-brush extension and the grafting density of the chains are now two more additional parameters influencing the brush properties, the problem becomes even richer than that of PE stars. In this review, we focus on PE stars, mentioning spherical polyelectrolyte brushes only tangentially and for those aspects of their experimentally determined properties that are relevant to PE stars. Recent reviews on brushes in general and on SPBs in specific can be found in Rühe *et al.* (2004) and Ballauff (2007), respectively.

This work is focused on recent progress from theory, simulations, and experiments pertaining to polyelectrolyte stars, for which the height of the polymer corona vastly exceeds the size of the central particle on which the polyelectrolytes are grafted, so that the latter can be effectively ignored. The emphasis of the review lies on the efforts to achieve a bridging of the length scales of the system. Accordingly, we commence with a microscopic description, in which the monomers, neutral and charged, as well as the counterions, are resolved as individual dynamical entities of the problem, and we describe the various approaches employed toward replacing those with their average values (density profiles) around the PE-star centers. Apart from the monomer profiles, the degree of adsorption and condensation of counterions are here the physically most relevant quantities and complementary approaches to this first step of coarse graining of the length scales are presented in Sec. II. The information gained is then employed to replace the whole PE star, with its surrounding halo of monomers and cloud of ions, with a single effective particle, i.e., its center, which interacts with other centers via a monomer- and a counterion-mediated effective interaction. Once more, different approaches to this end have been put forward. These distinct methods converge, however, toward a common picture, namely, that the counterion entropy plays the dominant role in determining the sought-for effective interaction. This second step in the coarse-graining procedure, which brings the description to a mesoscopic length scale, is presented in Sec. III. The last step proceeds naturally from the mesoscopic scale toward the macroscopic one, aiming at predictions pertaining to the phase behavior of the system as a whole and resting on information regarding the correlations between the effective particles in concentrated solutions. This aspect is presented in Sec. IV. Finally, in Sec. V we summarize and discuss the perspectives for future work in this field.

II. CONFORMATIONS OF MOLECULES IN DILUTE SOLUTIONS

A. Scaling theory for neutral stars

Daoud and Cotton investigated the different scaling regimes of neutral star polymers in good solvents (Daoud and Cotton, 1982). They adapted the so-called blob picture, originally introduced by de Gennes for linear polymer solutions (de Gennes, 1979) and applied this concept on star-shaped polymer systems. Many scaling approaches for polyelectrolyte stars are based on those ideas, as shown below. We first review the general concept of the blob picture of neutral star polymers.

In contrast to a solution of a homogeneous linear polymer solution, the polymer chains in a star-shaped architecture exhibit a strongly inhomogeneous density profile (see Fig. 1). This inhomogeneity is also reflected in different blob sizes expressed by the correlation length $\xi(r)$, which grows with increasing distance from the core region r. Assuming that the blobs are closely packed, one obtains for a star of f arms on purely geometrical grounds,

$$\xi(r) = rf^{-1/2}. \tag{1}$$

Daoud and Cotton distinguished now three different areas for the degree of swelling: the swollen region for monomer-center distances $r > r_1$, the unswollen region $r_2 < r < r_1$, and the core region for $r < r_2$ (see Fig. 1). For each of those regions there are different scaling laws for

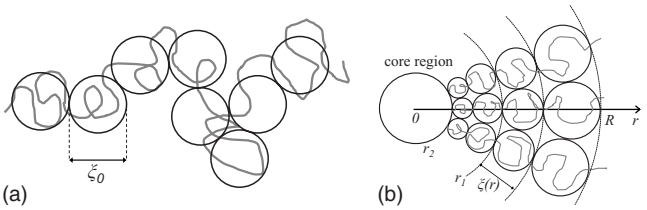

FIG. 1. Blob picture of a linear polymer chain (a) and of polymer chains in starlike architecture (b). The blob sizes are characterized by the correlation length of the monomers ξ_0 in the undisturbed polymer case and $\xi(r)$ for the polymer segments in the starlike architecture.

the correlation length $\xi(r)$, the number of monomers per blob $n(r)$, and the local monomer density within a blob $\rho(r)=n(r)/\xi^3(r)$. In the following, we focus only on the density. In the swollen region ($r>r_1$) the blob size $\xi(r)$ exceeds the distance over which the behavior of the chain is ideal. On such longer scales the chain is self-avoiding, which is expressed by the excluded volume parameter v. In this case, the size of the polymer segment scales with $\xi\sim v^{1/5}n^{3/5}$ (Flory, 1953; de Gennes, 1979). Using this relation and the geometrical condition [Eq. (1)], one readily obtains the monomer profile in the swollen region,

$$\rho(r) \sim r^{-4/3}f^{2/3}v^{-1/3}. \tag{2}$$

In the unswollen regime, $r_2<r<r_1$, the blob size is smaller, reaching the ideal chain limit. Here $\xi(r)=\xi_0=an^{1/2}$, where a is the monomer size, and the monomer density scales as

$$\rho(r) \sim r^{-1}f^{1/2}. \tag{3}$$

Finally, in the core regime, $r<r_2$, the blob size coincides with the monomer size and the local concentration $\rho(r)a^3$ reaches unity.

The center-to-end distance results from the integral of the monomer concentration over the whole star of functionality f and degree of polymerization of each chain N,

$$4\pi\int_0^{R_c}\rho(r)r^2dr = Nf. \tag{4}$$

By accounting for the three different scaling regimes of $\rho(r)$, Eq. (4) yields a scaling behavior for the star radius, namely,

$$R_c \sim \left[Nf+\frac{f^{3/2}a^6}{10v^2}+\frac{f^{3/2}}{6}\right]^{3/5}v^{1/5}\left(\frac{a}{f}\right)^{2/5}. \tag{5}$$

For long chains, i.e., $N\gg f^{1/2}v^{-2}$, the swollen chain contribution dominates, yielding

$$R_c(N,f) \sim N^{3/5}f^{1/5}\bar{v}^{1/5}a, \tag{6}$$

with $\bar{v}=va^{-3}$. In this case, the unswollen and core parts can be ignored. As can be seen, the spatial extension of the star is larger than that of an isolated chain with same degree of polymerization N due to the stretching of the chains caused by the star architecture.

B. Scaling theory for charged stars

For chargeable chains, the ion dissociation of the polymers increases the complexity of the system in many ways. On the one hand, the electrostatic interactions have a strong influence on the conformational behavior and, on the other hand, the role of the dissociated counterions needs to be addressed as well. These two physical aspects entail more parameters and length scales. They are, in particular, the Bjerrum length $\lambda_B=e^2/\epsilon kT=0.71$ nm for water at room temperature and the electrostatic screening length $\kappa^{-1}=(8\pi\lambda_B c_s)^{-1/2}$, with e the elementary charge, ϵ the dielectric constant, kT the thermal energy, and c_s the total ion (electrolyte) concentration in the PE solution. Because of these two additional parameters, various cases need to be distinguished. We explore one limit at which electrostatic effects dominate and one where they can be neglected. Those two limits are important and were analyzed by Pincus (1991) and in more detail by Borisov *et al.* (Borisov *et al.*, 1991, 1997; Zhulina *et al.*, 1991; Borisov, 1996; Klein Wolterink *et al.*, 1999). Recently, a comprehensive scaling analysis was used to calculate the conformational phase diagram of PE stars (Shusharina and Rubinstein, 2008).

In the following, we review the scaling approach of Borisov (1996), which is an extension of scaling analysis by Alexander (1977) and de Gennes (1987), originally put forward for planar brushes. For weakly charged polyelectrolyte stars in dilute solution, it is assumed that the counterions are released and homogeneously distributed in solution. In such cases, counterion entropy can be ignored and the electrostatic contributions are dominant. In a mean-field approach, the free energy of the star consists only of a Coulomb contribution $U_{\rm Coul}$ and of elastic chain contributions $\tilde{\mathcal{F}}_{\rm el}$. The Coulomb repulsion between the chains within the star is given by

$$\frac{U_{\rm Coul}}{kT} \approx \frac{\lambda_B(\alpha fN)^2}{R}, \tag{7}$$

where α is the fraction of charged monomers per chain and R is the equilibrium size of the star. This repulsion is compensated by the elasticity of f self-avoiding stretched chains, given by (Pincus, 1977; de Gennes, 1979)

$$\frac{\tilde{\mathcal{F}}_{\rm el}}{kT} \approx f\left(\frac{R}{R_c(N,1)}\right)^{5/2}, \tag{8}$$

where $R_c(N,1)$ is taken from Eq. (6). Equation (8) is based on a scaling relation for the relative size ratio $R/R_c(N,1)$ as a response to a tension force that is caused here by electrostatics (Pincus, 1977).

Minimization of the sum of both energy contributions yields

$$R \approx Na\alpha^{4/7}\bar{v}^{1/7}f^{2/7}u^{2/7}, \tag{9}$$

with $u\equiv\lambda_B/a$. Compared to the scaling behavior of a neutral star [Eq. (6)], the radius scales stronger with the degree of polymerization N and the functionality f; this points to a stronger stretching of the chains. The scaling

result in Eq. (9) is only valid if the star is weakly charged, i.e., the average distance between neighboring chains is smaller than the Bjerrum length λ_B. For stronger-charged PE stars, counterions are attracted and absorbed within the stars' coronae. Those counterions screen the Coulomb potential between the chains and the Coulomb energy can be ignored. Now, however, the entropy or the osmotic pressure of trapped counterions becomes important. For highly charged PE stars, the elastic energy of the chains, $\tilde{\mathcal{F}}_{\rm el}$ from Eq. (8), is then compensated by free-energy contribution of the counterion entropy,

$$S_{\rm osm} = -k\alpha f N\left[\ln\left(\frac{3\alpha f N}{4\pi R^3}\right) - 1\right]. \tag{10}$$

Minimization of the total free energy $\tilde{\mathcal{F}}_{\rm el} - TS_{\rm osm}$ with respect to R leads to the determination of the size of the so-called osmotic star as

$$R \approx Na\alpha^{2/5}\tilde{v}^{1/5}. \tag{11}$$

R turns out to be independent of f in this case because both the elastic contribution [Eq. (8)] and the entropic one [Eq. (10)] yield upon differentiation with respect to R a common f factor that drops out of the minimization requirement. In contrast, the size of neutral star polymers and that of unscreened PE stars feature a dependence on f [see Eqs. (6) and (9), respectively].

The crossover between a Coulomb star and an osmotic star has been estimated using scaling arguments. If $\alpha f N\lambda_B/R(f) \ll 1$, counterion absorption can be neglected, and Coulomb repulsion between chains is important. From this criterion, one can estimate a crossover functionality $f_\times = \alpha^{-3/5}u^{-1}v^{-1/5}$. Above this limit, the stars are osmotic and the scaling ratio [Eq. (11)] is valid (Borisov, 1996). The results are based on the assumption that counterion condensation on the chains can be neglected; we, nevertheless, show below that this effect is very important at least as far as the *interaction* between two stars is concerned. In fact, Shusharina and Rubinstein (2008) recently incorporated counterion condensation into the scaling analysis by replacing $\alpha f N \to \tilde{\beta}\alpha f N$ with $\tilde{\beta}$ the fraction of noncondensed ions. This fraction is estimated through the Manning condition (Manning, 1969) for condensation $\tilde{\beta} \approx 1/u^2\alpha$ for $u^2\alpha > 1$. Using the counterion condensation, more scaling regimes are found, leading to an expanded blob picture of PE stars (Shusharina and Rubinstein, 2008).

C. Variational free-energy approach

Apart from the scaling analysis of PE stars, there are mean-field approaches for predicting conformational properties. In the aforementioned scaling model, it was assumed that either the counterions are completely dissociated into the solution or they are completely trapped inside the PE star. In reality, there are fractions of free and confined counterions. Consequently, the PE star bears a net charge that interacts with its environment.

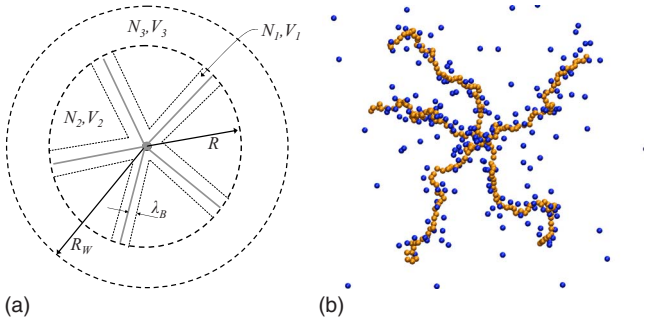

FIG. 2. (Color online) Conformations of polyelectrolyte stars. (a) Sketch of a PE star consisting of $f=5$ stretched arms and radius R inside a spherical Wigner-Seitz cell of radius R_W. There are three different states $i=1,2,3$ for the counterions, with populations N_i. In particular, N_1 are condensed within tubes of total volume V_1, N_2 are trapped in the volume V_2 inside the star, and N_3 counterions are free in the outside volume V_3 (Jusufi *et al.*, 2002a, 2002b). (b) Simulation snapshot of a $f=5$ PE star with $N=50$ monomers per arm and a charge fraction $\alpha=1$. Connected spheres denote charged monomers, whereas the star counterions are shown as disconnected spheres.

Furthermore, the entropic contribution of the confined counterions $S_{\rm osm}$ is modified due to the changed number of counterions that are located inside the star. In Eq. (10), it is assumed that all counterions are absorbed. The number of confined ions is, in addition to the radius of the PE star, an important quantity for the conformational behavior of PE stars.

For dilute PE star solutions, the Wigner-Seitz cell model is a convenient framework within which the free energy can be estimated. In this approach, it is assumed that interactions between PE stars in solution can be neglected; at the cell boundary the electric field induced by the charged PE star vanishes. Consider a single star in a spherical cell of radius R_W, whose size depends on the density $\rho = N_{\rm s}/V$ of $N_{\rm s}$ stars in the macroscopic volume V. In particular, $R_W = (4\pi\rho/3)^{-1/3}$. In Fig. 2(a), a five arm star within a Wigner-Seitz cell is sketched, whereas in Fig. 2(b) a simulation snapshot of a five arm PE star with all of its monomers being charged is shown to demonstrate the stretching of the arms and justify the theoretical modeling of the latter as rigid rods. At sufficiently high bare valency of the star, $Q_b = \alpha f N$, counterions are trapped inside the star, similar to the above scaling analysis of the osmotic star. As a result, the net valency of the star is $Q^* < Q_b$. Due to overall charge neutrality, the outside environment must have a net charge of magnitude $Q^*|e|$, which stems from the free counterions. Inside the star, electrostatic interactions between neighboring chains are neglected again, which is true as long as $|Q_b|\lambda_B/R \gg 1$.

The model is an extension of that introduced by Klein Wolterink *et al.* (1999). It accounts for two important aspects: first, counterion condensation has been taken into account, and second, the trapped noncondensed counterions possess an inhomogeneous distribution that

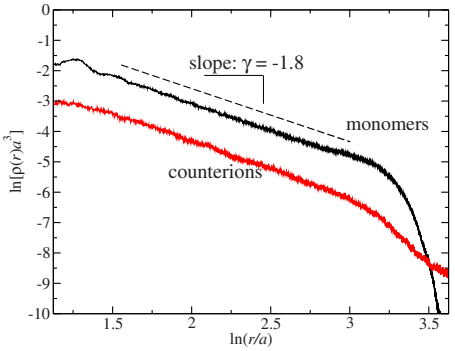

FIG. 3. (Color online) Double logarithmic plot of density profiles of monomers (black line) and counterions [red (gray) line] $\rho(r)$ as a function of the distance r from the central monomer. The results stem from MD simulations of a star which consists of $f=10$ arms with degree of polymerization, $N=50$, and a charge fraction $\alpha=1/3$. The slope indicates strong stretching of the arms, close to the full stretching limit, in which $\rho(r)\sim r^{-2}$ (Jusufi *et al.*, 2002a, 2002b).

decays as $\sim r^{-2}$ from the star center (see Fig. 3). The first aspect gives rise to an additional counterion state, thus we call this the *three-state model*, to distinguish it from the *two-state model* of Klein Wolterink *et al.* for which the counterions are either trapped within the star or free in the solution. This multistate model for the counterions has been already introduced for solutions of linear polyelectrolytes (Kramarenko *et al.*, 2000). As can be seen from the sketch in Fig. 2(a), there are N_1 counterions localized in cylinders around each stretched arm, N_2 noncondensed counterions inside the star in a volume V_2, and finally N_3 free counterions outside the star in the shell volume V_3. It has been confirmed via extensive molecular dynamics (MD) simulations (see Fig. 3), which the confined counterion density decays as $\sim 1/r^2$ with the distance r from the star center, similar to the monomer density profile. The oscillations of the monomer profile are caused by packing effects around the core. The measured profile decays with $\rho(r)\sim r^{\gamma}$, $\gamma\cong -2$ due to stretching, which is stronger than the neutral star ($\gamma=-1.33$) compared with Eq. (2). The asymptotic limit for fully stretched chains is indeed $\gamma=-2$ (Pincus, 1991; Borisov and Zhulina, 1997). The $1/r^2$ decay of the density profile has been confirmed by several studies, encompassing computer simulations (Jusufi *et al.*, 2002a, 2002b; Roger *et al.*, 2002; Jusufi, 2006) and experiments (Groenewegen, Egelhaaf, *et al.*, 2000; Groenewegen, Lapp, *et al.*, 2000; Dingenouts *et al.*, 2004). It is evident that one can tune the density profile, going from coiled chains (neutral star polymers) to fully stretched ones, by gradual increase of the charge ratio α (Borisov and Zhulina, 1997).

In what follows, we review the main steps for the determination of the equilibrium values of N_i $(i=1,2,3)$ and the star radius R (Jusufi *et al.*, 2002a, 2002b). Those quantities are obtained from minimization of a variational free energy, which is comprised of electrostatic contributions, entropic terms of the counterions, and Flory-like chain contributions. The electrostatic energies account for the interaction between the stars of net charge Q^*e with its counterion environment that carries the opposite charge $|e|N_3$ to fulfill the electroneutrality requirement. Note that $\Sigma_{i=1}^{3}N_i=\alpha fN=|Q_b|$. Using a Hartree-type mean-field approximation, the electrostatic term is calculated through

$$U_{\mathrm{H}}=\frac{1}{2\epsilon}\int\int d^3r d^3r'\frac{\varrho(\boldsymbol{r})\varrho(\boldsymbol{r}')}{|\boldsymbol{r}-\boldsymbol{r}'|}, \tag{12}$$

where $\varrho(\boldsymbol{r})$ is the local charge density. Accounting for the $1/r^2$ decay inside the star and assuming a homogeneous distribution of charges outside the star, the total charge density is given by

$$\frac{\varrho(\boldsymbol{r})}{|e|Q_*}=\frac{\Theta(R-r)}{4\pi Rr^2}-\frac{\Theta(r-R)\Theta(R_W-r)}{V_3},$$

with the Heaviside step function $\Theta(x)$. Recent self-consistent field calculations justify the use of a homogeneous profile of counterions outside the star (Leermakers *et al.*, 2008). The calculation of Eq. (12) can be expressed in closed form (Jusufi *et al.*, 2002b) as a series of analytical functions and has been reported by Jusufi *et al.* (2002b).

Equation (12) is, evidently, a mean-field approximation that ignores all correlation effects. The strongest charge-charge correlations appear between the charged monomers along the chains and the counterions that are cylindrically condensed along the PE arms. This counterion condensation inside tubes around the chains of length R and radius λ_B is accounted for by an electrostatic correlation term, which expresses the gain of electrostatic energy if counterions are condensed close to the chains (Jusufi *et al.*, 2002b),

$$U_c=-kTN_1\frac{\lambda_B}{z_m}, \tag{13}$$

with $z_m=(1/2)\sqrt{\lambda_B^2+y_m^2}$ the average chain-counterion separation. This contribution is proportional to the number of cylindrically condensed counterions along the rods N_1 and its strength is further determined by the typical counterion-chain separation z_m (Jusufi, 2002b). Here y_m is the average distance between charged monomers along each chain, i.e., $y_m=R/N\alpha$.

For each of the three counterion states the corresponding entropic contributions are given by

$$S_i=-k\int_{V_i}d^3r\rho_i(r)\ln\rho_i(r), \tag{14}$$

with $i=1,2,3$ and $\rho_i(r)$ the ion density distributions. The condensed and free counterion distributions are homogeneous inside their volumes, i.e., $\rho_1=N_1/V_1$ and $\rho_3=N_3/V_3$. The confined noncondensed counterions exhibit a r^{-2} decay, their density normalized by the condition $\int_{V_2}d^3r\rho_2(r)=N_2$. The corresponding volumes are $V_1=f\pi R(\lambda_B^2-a^2)$, accounting for the hollow tubes around each chain, $V_2=(4\pi/3)R^3-f4\pi R\lambda_B^2$ for the

residual volume of the interior of the star, and $V_3=(4\pi/3)(R_W^3-R^3)$ the outer shell volume.

Finally, the chain contributions are comprised of an elastic term

$$\frac{\mathcal{F}_{\rm el}}{kT}=\frac{3fR^2}{2Na^2} \tag{15}$$

and a self-avoidance Flory term

$$\frac{\mathcal{F}_{\rm Fl}}{kT}=\frac{3v(fN)^2}{8\pi R^3}. \tag{16}$$

These are added to Eqs. (12) and (13) and $-T\Sigma_{i=1}^3 S_i$ of Eq. (14) to obtain the total variational free energy $\mathcal{F}(R;\{N_i\})$, which has to be minimized with respect to the star radius R and the counterion populations N_i, $i=1,2,3$ under the neutrality constraint $\Sigma_{i=1}^3 N_i=\alpha fN$. Note that the chain contributions [Eqs. (15) and (16)] are now incorporated in the minimization procedure, in contrast to the scaling analysis in Sec. II.B, where the scaling relation [Eq. (8)] has been used from the outset.

In Fig. 4 results for a star with $\alpha=1/3$ [Fig. 4(a)] and $\alpha=1/2$ [Fig. 4(b)] are shown for the f dependence of the fraction of trapped and condensed counterions $(N_1+N_2)/Q_b$ and N_1/Q_b, respectively. Both fractions increase with arm number f and converge at high functionality; the star is almost completely neutralized in this limit. In the intermediate regime, the three-state model overestimates MD simulation results (Jusufi *et al.*, 2002a, 2002b) (cf. solid lines with symbols in Fig. 4). A better description is achieved by the simpler two-state model (dashed line) although the latter does not account for counterion condensation (Klein Wolterink *et al.*, 1999). The fraction of condensed counterions increases as well (dashed-dotted line and squares in Fig. 4). The simulation results seem to converge to the Manning limit, $1-1/(u^2\alpha)$, while the theoretical curve from the three-state model increases further and overestimates the simulation results. Keeping in mind that it is challenging to capture condensation effects over a broad f regime, the curves demonstrate the nonconstant characteristic of condensation on chains inside the star.

In Fig. 5 we show the calculated radius R as a function of the degree of polymerization N. The theoretical curve is compared with the variational free-energy calculation of the two-state model, which assumes a homogeneous counterion density profile inside the stars and no counterion condensation (Klein Wolterink *et al.*, 1999). The N dependence of both theories is almost identical. A power-law fit of the MD results yields $R\sim N^{0.98}\approx N$, in excellent agreement with the scaling prediction for an osmotic star [Eq. (11)]. The f dependence of R is plotted in Fig. 6 for a star with $\alpha=1/3$ [Fig. 6(a)] and $\alpha=1/2$ [Fig. 6(b)]. The latter shows a nonmonotonic behavior above $f>5$: at $f\approx 20$ the three-state model predicts a minimum, which is confirmed by simulation results (Jusufi, 2006). The nonmonotonic behavior of $R(f)$ stems from the pronounced nonmonotonic behavior of the ratio of condensed to noncondensed counterions inside the star, as can be read off from the gap between the solid and dashed-dotted lines in Fig. 4(b). This behavior is not pronounced for the weaker charged star shown in Fig. 4(a). The two-state counterion model overestimates $R(f)$, which demonstrates the importance of accounting for counterion condensation in the three-state model, despite its nonconstant characteristic. Here one should note that the condensed counterions are still osmotically active. In reality, only a small fraction of counterions are strictly condensed, so that they can be viewed as osmotically deactivated. Accounting for this "strict condensation" would further reduce the f dependence of the radius R, however, at the expense of introducing additional fit parameters or further states of counterions, which would complicate the theory. In Fig. 6, power-law fits of the simulation results are shown as well. The fits yield $R\sim f^{0.04}\approx 1$ [Fig. 6(a)] and $R\sim f^{0.02}\approx 1$ [Fig. 6(b)] and are in excellent agreement with the scaling prediction for an osmotic star [Eq. (11)]. The in-

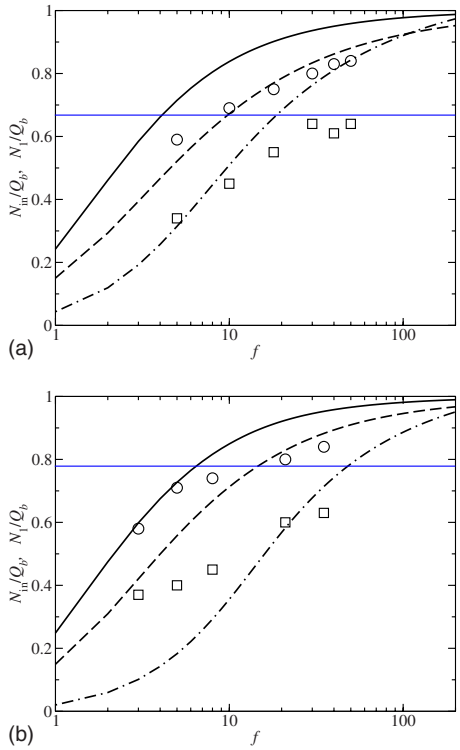

FIG. 4. (Color online) The fraction of trapped counterions $N_{\rm in}/Q_b$ (where $N_{\rm in}=N_1+N_2$) plotted vs the star functionality f. The simulation results, denoted by the circles, are compared with variational free-energy calculations of the three-state model, black solid line (Jusufi *et al.*, 2002a, 2002b), and of the two-state model, black dashed line (Klein Wolterink *et al.*, 1999). The fraction of condensed counterions N_1/Q_b calculated from simulations (squares) and that from the three-state model (dash-dotted line) are shown as well. The Manning condition for the fraction of condensed counterions is $1-1/(u^2\alpha)$ and is denoted by the horizontal line. (a) Star with degree of polymerization per arm $N=50$, $\alpha=1/3$, and cell radius $R_W=55.83a$, simulation results from (Jusufi *et al.*, 2002a, 2002b). (b) Star with $N=60$, $\alpha=1/2$, and $R_W=99.26a$.

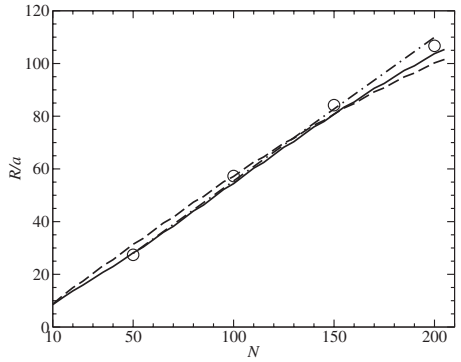

FIG. 5. The star radius R vs the degree of polymerization N for a star with functionality $f=10$, $\alpha=1/3$, and cell radius $R_W=136.48a$. The simulation results, denoted by the circles (Jusufi *et al.*, 2002a, 2002b), along with a power-law fit of the same (dash-dotted line), are compared with variational free-energy calculations of the three-state model (solid line) (Jusufi *et al.*, 2002a, 2002b) and the two-state model (dashed line) (Klein Wolterink *et al.*, 1999).

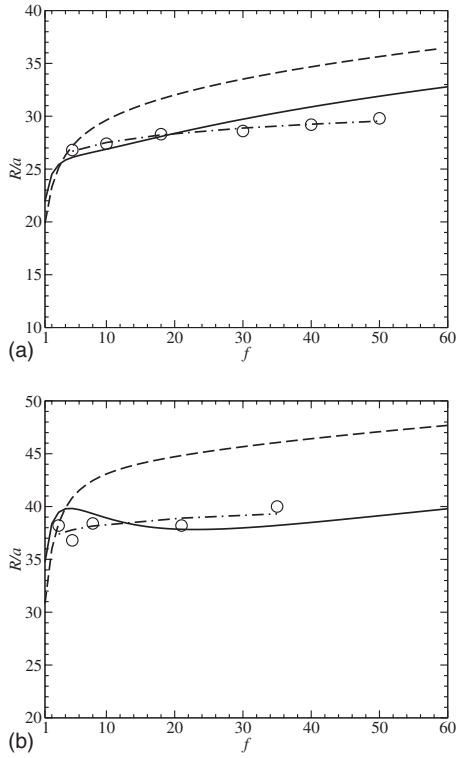

FIG. 6. Sizes of polyelectrolyte stars. The star radius R vs functionality f. The simulation results, denoted by the circles, along with a power-law fit of the same (dash-dotted line), compared with variational free-energy calculations of the three-state model (solid line) (Jusufi *et al.*, 2002a, 2002b), and the two-state model (dashed line) (Klein Wolterink *et al.*, 1999). (a) Star with degree of polymerization per arm $N=50$, $\alpha=1/3$, and cell radius $R_W=55.83a$, simulation results from Jusufi *et al.* (2002a, 2002b) (b) Star with $N=60$, $\alpha=1/2$, and $R_W=99.26a$, simulation results from Jusufi, 2006.

crease for small chain numbers, $f<10$, shows the nonosmotic behavior of the star; beyond that limit the star radius is practically f independent. This result reflects the dominant effect of the counterion entropy at high f. The osmotic pressure in the star interior induces stretched arms (Borisov *et al.*, 1991; Pincus, 1991). The Coulomb interactions are essentially screened due to pronounced counterion condensation. Using the above theory, which is valid particularly for osmotic stars, good agreement with MD results is achieved for stars with $f\gtrsim 10$ and $\alpha\gtrsim 1/4$ (Jusufi *et al.*, 2002b).

Comparing the quality of the three-state model with that of the two-state counterion model, we conclude that both models give a reasonable description of the simulation data. The latter is better suited to predict the effective charge, while the former predicts the size well. Note, however, that the results for the relative effective charges Q^*/Q_b from the three-state and from the two-state theory converge to each other at high functionality f (see Fig. 4). In contrast, the disparity in the predictions of the two models for the radii persists in this limit (see Fig. 6). This is important for spherical polyelectrolyte brushes, where a brush consists of thousands of chains. For these systems, the three-state model is expected to give reasonable results for both the effective charge and the radius. Another important aspect is the relevance of the models for the effective interaction between stars. The use of a homogeneous counterion profile leads to a erroneous force between the objects. The three-state counterion model, on the other hand, yields an increasingly repulsive force upon pressing two stars together at the right scale. This force would be much too strong if counterion condensations were not taken into consideration. We discuss this point in Sec. III.

D. Influence of salt

The addition of salt has a significant impact on the conformational behavior of PE stars. In the osmotic regime, the electrostatic interaction between the chains is already screened by the star's own counterions. The osmotic pressure induced by trapped counterions inside the star is not balanced by the exterior osmotic pressure from ions outside the star. The corresponding force imbalance is mainly canceled by elastic chain forces compare the corresponding free-energy contributions [Eqs. (15) and (10)]. Upon addition of salt, the osmotic pressure difference between the interior and exterior of the star decreases. Therefore, the required elastic chain force $F_{\rm el}$ is smaller, which, in turn, reduces the star size. However, the deswelling is expected to be only pronounced when the added-salt concentration c_s exceeds the counterion concentration of the interior of the star.

Borisov and Zhulina incorporated these considerations into a scaling model for the added-salt case (Borisov and Zhulina, 1998). The ion concentrations inside and outside the star are governed by the Donnan equilibrium,

$$\frac{c_{\rm in}^-}{c_{\rm out}^-}=\frac{c_{\rm out}^+}{c_{\rm in}^+}, \tag{17}$$

with c_x^j the concentrations of coions ($j=-$) and counterions $j=+$, distinguished by being inside ($x=$in) or outside

(x=out) the star. Without loss of generality, we assume that the bare charge of the PE star is negative. Further, we concentrate on the case in which the added-salt ions dominate over the stars' own counterions, for which case we expect the star to be electrically neutral. Accordingly, electroneutrality conditions are applied separately in the interior and the exterior of the star, yielding $\alpha c_m + c_{\text{in}}^- = c_{\text{in}}^+$, with the monomer density $c_m = 3fN/4\pi R^3$, and $c_{\text{out}}^- = c_{\text{out}}^+$. Assuming that the ion concentration outside the star is equal to the bulk salt concentration c_s, all c_x^j are readily obtained. In particular, for the highly salted solution, $c_s \gg \alpha c_m$, the result reads $c_{\text{in}}^{\pm} \cong c_s \pm (\alpha c_m)/2 + (\alpha c_m)^2/8c_s$.

It is convenient to consider directly the ideal osmotic pressure of each ion species in its corresponding space, instead of the entropy, in order to eliminate the volumes. The pressure difference between the star interior and exterior is then

$$\frac{\Delta\Pi}{kT} = \sum_{j=-,+} (c_{\text{in}}^j - c_{\text{out}}^j). \tag{18}$$

Introducing the expressions for $c_{\text{in}}^{\pm}$ quoted above and using $c_{\text{out}}^{\pm} = c_s$, we see that the leading and linear terms in the expansion cancel, leaving a quadratic dependence of the pressure difference on the quantity αc_m, namely, $\Delta\Pi/kT \cong (\alpha c_m)^2/4c_s$. This is the same result already obtained for planar polyelectrolyte brushes (Witten and Pincus, 1987); note that $c_m = c_m(R)$ by definition. The corresponding osmotic pressure force $4\pi\Delta\Pi R^2$ is balanced by the elastic chain force $-\partial\mathcal{F}_{\text{el}}/\partial R$ as given by Eq. (15). Under the assumption that the salt concentration exceeds the counterion concentration inside the star ($c_s \gg \alpha c_m$), we obtain a scaling result for the size of the star,

$$R \approx N^{3/5} f^{1/5} (\alpha^2 c_s^{-1} a^{-3})^{1/5} a. \tag{19}$$

The osmotic star size shrinks with increasing salt concentration c_s. Note the similarity to the neutral star scaling results [Eq. (6)]. By direct comparison, we can identify an effective excluded volume v_{eff} given by $v_{\text{eff}} = \alpha^2/c_s$, which explicitly depends on the salt concentration c_s. It is physically intuitive that v_{eff} decreases with c_s (screening) and increases with the charging fraction α. Alternatively, one can define the effective excluded volume through the Debye screening parameter as $v_{\text{eff}} = 8\pi\lambda_B/\kappa^2$ (de Gennes, 1979), where $\kappa = \sqrt{8\pi\lambda_B c_s}$ and $\alpha = 1$. Using the Witten-Pincus form for the osmotic pressure (Witten and Pincus, 1987), the scaling form [Eq. (19)] is readily obtained [see Pincus (1991) for further details].

Within this scaling approach, a series of simplifications has been made. Again, counterion condensation has been neglected and the assumption of homogeneous profiles inside the star is only valid for $c_s \gg \alpha c_m(R_0)$. Furthermore, we showed that the effective charge of the star is small for larger stars $f \gg 1$ but in the intermediate regime this charge is still significant (see Fig. 4). It can be expected that the effective charge Q^* will gradually decrease upon addition of salt. This quantity is important

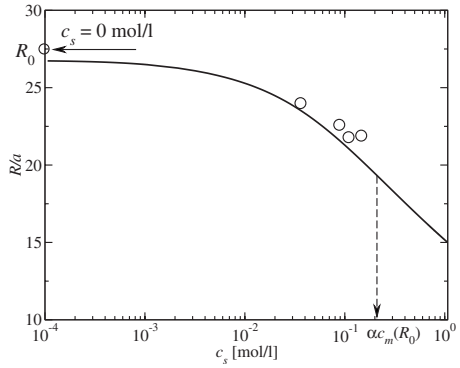

FIG. 7. Theoretical prediction, solid line, of the salt dependence of a ten arm star with $N=50$, $\alpha=1/3$, compared with simulation results, circles (Jusufi *et al.*, 2002b). Above the threshold $c_s > \alpha c_m(R_0)$, the scaling relation is $R \sim c_s^{-0.16}$.

for the determination of the effective interaction between stars both for overlapping and for nonoverlapping interstar separations, as demonstrated in Sec. III. The three-state model, described in Sec. II.C, has to be extended to the case $c_s \neq 0$, allowing for the calculation of the effective charge and the radius as functions of salt concentration c_s (Jusufi *et al.*, 2002b). In the following we focus on the salt dependence of the star size. Addition of salt ions results in the appearance of further entropic terms and modifications of Eq. (14). The entropic contributions to the free-energy must be modified by replacing the trapped noncondensed ion number $N_2 \to N_{\text{in}}^+ + N_{\text{in}}^- - N_1$ and the free ion number $N_3 \to 2N_s + \alpha fN - (N_{\text{in}}^+ + N_{\text{in}}^-)$, where $N_{\text{in}}^j = c_{\text{in}}^j V_2$ and $N_{\text{out}}^j = c_{\text{out}}^j V_3$ ($j=+,-$). Instead of using the Donnan equilibrium [Eq. (17)], we minimize the corresponding total free-energy with respect to R, N_{in}^+, N_{in}^-, and N_1 (number of condensed counterions). The numerical minimization yields $N_{\text{in}}^- = 0$. The almost complete exclusion of coions from the star interior has been confirmed by MD simulations, in which it was found that less than 5% of the salt coions penetrate the star (Jusufi *et al.*, 2002b).

In Fig. 7 the salt dependence of the star radius R is shown for a PE star with $f=10$, $N=50$, and $\alpha=1/3$. Compared are predictions from variational free-energy calculations with simulation results (Jusufi *et al.*, 2002b). Apart from the value at $c_s \approx 0.15$ mol/L, the simulation results confirm the decrease of R with salt concentration. The comparison proves that the onset of the deswelling is reached before the theoretical threshold $c_s \approx \alpha c_m(R_0)$, indicated by a dashed arrow. Above that limit, a power-law fit of the theoretical curve yields $R \sim c_s^{-0.16}$, which marks a slightly weaker decay than the scaling relation $R \sim c_s^{-0.2}$ of Eq. (19).

We finally turn to the case of added multivalent salt ions. In recent years, interest in these systems has significantly increased due to the ions' strong impact on conformational and phase behavior of PE brushes and PE stars. Various theoretical approaches, such as scaling concepts (Zhulina *et al.*, 1999) or Poisson-Boltzmann theory (Santangelo and Lau, 2004), have been applied to

investigate specifically the conformational behavior of such systems in the presence of multivalent counterions. Experimental studies (Mei *et al.*, 2006; Plamper *et al.*, 2007) demonstrated that minute concentrations of multivalent ions induce a collapse of the stars in particular for trivalent counterions (valency $q=3$). The collapse has two origins: first, adding multivalent ions to a solution leads to an ion exchange. In the osmotic regime, the exchange can be well described by a Donnan equilibrium (Zhulina *et al.*, 1999; Mei *et al.*, 2006): the ion density in the star is reduced by a factor of q, leading to a decrease of the osmotic pressure inside the star. This reduction is not sufficient to describe the complete collapse observed in experiments or simulations. A further reduction is induced by strong ion correlations on the PE chains, which is the second origin of the collapse. Compared to monovalent ions, multivalent ones are virtually deactivated, i.e., their contribution to the osmotic pressure is negligible.

A good description of the collapse of the star in the presence of multivalent counterions is offered by the following model. Here we focus on the salt-free case (Mei *et al.*, 2008) although the model is also suitable for the added-salt case for which it has been demonstrated that the model describes quantitatively experimental results (Mei *et al.*, 2006). We consider again the chain forces F_{ch} obtained from the derivatives of Eqs. (15) and (16) with respect to the radius R,

$$F_{\mathrm{ch}} = -\frac{3kTfR}{Na^2} + vkT(fN)^2\frac{9}{8\pi R^4}. \tag{20}$$

These forces balance the osmotic pressure force originating from the counterions, i.e., monovalent and multivalent ones,

$$F_p^i = kT(\eta^+ c_{\mathrm{in}}^+ + \eta^{q+} c_{\mathrm{in}}^{q+})4\pi R^2, \tag{21}$$

where c_{in}^+ and c_{in}^{q+} are concentrations of monovalent and multivalent counterions (valency q), respectively. We introduce two parameters η^+ and η^{q+}, which account for osmotic activity inside the star, hence $0 \leqslant \eta^i \leqslant 1$ with $i=+,q+$. In the following, η_i are used as fit parameters, resulting from fitting the radius of a PE-star system where only one type of counterion is present. We assume that all counterions are trapped (there are no coions in the absence of salt) as in the scaling analysis above, i.e., $c_{\mathrm{out}}^+ = c_{\mathrm{out}}^{q+} \equiv 0$. The radius R is obtained by requiring that the total force, expressed as the sum of Eqs. (20) and (21), vanishes. In a recent study, this approach was applied on spherical polyelectrolyte brushes (SPBs), which are very similar to PE stars, but with a core of nonvanishing size. Here the effect of the core radius r_c needs to be implemented into Eqs. (20) and (21) [see Mei *et al.* (2008) for details]. In Fig. 8, the relative brush thickness per monomer $(R-r_c)/Na$ is plotted as a function of the ratio of the overall ion concentration c^{q+}/c^+ for a spherical brush with $r_c=6a$, $f=40$, $N=30$, and $\alpha=1$. The values of the fit parameters are $\eta^+=0.8$, $\eta^{2+}=0.3$, and $\eta^{q+}=0$ for $q \geqslant 3$. They were obtained from fitting the cases where only one ion component is present, i.e., at $c^+=0$ and $c^{q+}=0$ and kept constant for all ratios c^{q+}/c^+. The agreement of the theory with MD data is good and describes the collapse of the brush quantitatively. The theory is also in quantitative agreement with experiments of SPBs that carry bare charges of the order of 10^5–10^6 elementary charges (Mei *et al.*, 2006). The parameter values are the same as presented here. It should be noted that $\eta^+=0.8$ is much larger than the Manning estimate $\tilde{\beta}=1/u^2\alpha \approx 0.1$ (see Sec. II.B), which means that more monovalent ions are osmotically active. The higher value supports the condensation picture schematically shown in Fig. 2, where the ions are condensed within tubes around the chains (see Sec. II.C). The term "chain localization" is therefore more suitable for monovalent ions. Those ions are, despite their localization, still osmotically active. Upon valency increase, the osmotic degree, expressed in η^i, decays to 0.3 for $q=2$ and to 0 for $q \geqslant 3$. Thus, at high valencies, the ions are strictly condensed and virtually "switched off." This picture has been confirmed by MD simulations in which ion-chain correlations were measured (Mei *et al.*, 2008).

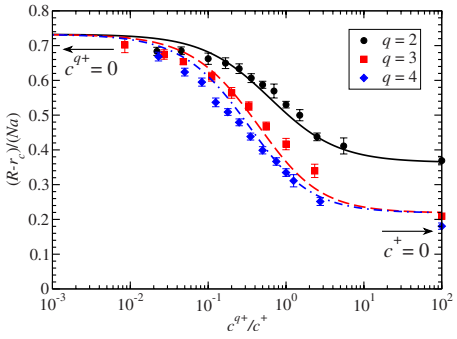

FIG. 8. (Color online) Relative brush thickness for a spherical polyelectrolyte brush with core size $r_c=6a$, $f=40$, $N=30$, and $\alpha=1$. The concentration ratio of multivalent to monovalent ions c^{q+}/c^+ is varied. Compared are theoretical results (lines) with data obtained from MD simulations (symbols) for systems with valencies $q=2$ (spheres and solid line), $q=3$ (squares and dashed line), and $q=4$ (diamonds and dash-dotted line). From Mei *et al.*, 2008.

It is remarkable that the above theory, despite its simplicity, can describe more complex systems. Computer simulations of spherical polyelectrolyte brushes that are mixed with oppositely charged linear polyelectrolytes of same chain length N as the ones grafted on the core show a collapse due to absorption of linear polyions (Ni *et al.*, 2008). The mechanism is the same: once the polyions are absorbed by the brush, the osmotic pressure decreases and the brush collapses. The theory describes the collapse in a similarly quantitative manner as for the simple system shown in Fig. 8. However, upon further addition of polyions ($qc^{q+} > c^+$), a reswelling occurs, accompanied by a charge inversion (Grosberg *et al.*, 2002). Those effects are naturally not captured by the simple model above; it remains an open task to incorporate local correlation effects in a theoretical model.

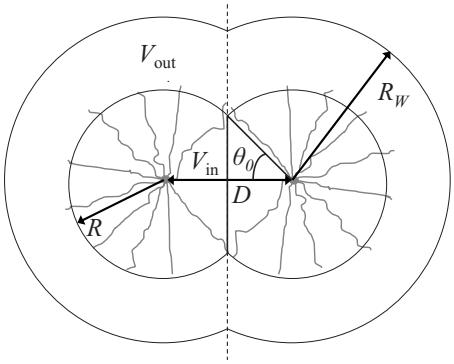

FIG. 9. Two stars of radius R at center-to-center distance D. At the bisecting plane the chains retract from each other. The surface section $\mathcal{S}$ where the two stars meet is indicated by a solid black line in the bisecting plane (dashed line). The two stars are within a cell of a fused double-sphere shape of radius R_W. The volume of the two fused stars is $V_{in}(D)=2\Omega(D)$ and that of the shell outside the stars is $V_{out}(D)$.

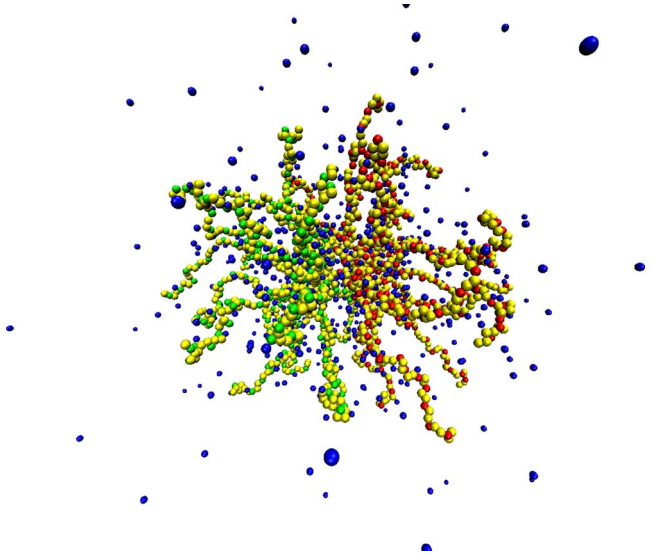

FIG. 10. (Color online) Simulation snapshot of two PE stars with $f=18$ arms and $N=50$ monomers per arm each at a center-to-center separation $D\approx 0.2R$. The light-colored, connected spheres denote neutral monomers, whereas the dark, connected ones denote charged monomers on each star. Disconnected spheres are the star counterions. Note the retraction of the arms of each star toward the half-space on which the star lies.

III. EFFECTIVE INTERACTIONS BETWEEN PE STARS

In the preceding section we identified the dominant physical mechanisms that determine the conformational behavior of a *single* star. Here we turn our attention to the *effective interaction* between the centers of two PE stars, defined as the constrained free energy of the two, obtained by averaging over all other degrees of freedom involved but keeping the centers fixed at separation D (Likos, 2001). In the osmotic regime, which is already reached for $f\gtrsim 10$ and $\alpha\gtrsim 1/4$, the entropic contribution of the confined counterions to the free energy is the key quantity both for the star conformation and for interstar interactions. Indeed, we showed quantitatively that condensation or chain localization of counterions within the star and a $1/r^2$-density profile of the remaining ions inside the star is important for the conformation; we now take advantage of this fact to describe theoretically the aforementioned effective interaction $V_{eff}(D)$ between two such stars. A quantitative understanding of the interaction enables us to make the decisive *coarse-graining* step from a microscopic (monomer and ion resolved) to a coarse-grained (mesoscopic) description of PE stars. The latter is perfectly suited to be treated by means of liquid-state theories, leading to the determination of structural and phase behavior, which is the subject of Sec. IV.

A. The role of osmotic pressure forces

Since the osmotic pressure of confined counterions determines the conformational properties of the stars, it must also play an important role when two stars are brought together within a separation D that is smaller than their diameter $\sigma=2R$. This is mainly due to the changes in the star volume available to the trapped counterions (see Fig. 9). In this interaction model, the chains retract from each other avoiding interdigitation. This picture has been confirmed by simulations (Jusufi *et al.*, 2002a, 2002b; Wang and Denton, 2005) (see Fig. 10), and experiments (Korobko *et al.*, 2004; Wittemann *et al.*, 2005). Pincus estimated the interaction force using scaling arguments (Pincus, 1991). He argued that the local osmotic pressure of the trapped counterions in the interior of a star is $\Pi(r)=kTc_{in}(r)$, with $c_{in}(r)=A/r^2$ the counterion density profile inside the star, which follows the same $1/r^2$ decay as the monomer profile due to the tendency of the system to achieve local charge neutrality. The constant A is received by the normalization condition,

$$\int_\Omega \frac{A}{r^2} d^3r = \alpha f N, \tag{22}$$

where Ω is the volume of a single star. Evidently, $\Omega=\Omega(D)$ since the spherical star is "chopped" at the bisecting plane if a second one is held fixed at a separation $D<\sigma$ from it. For simplicity, all counterions are assumed to be confined inside the star volume Ω; counterion condensation is not considered at this point.

The force $\boldsymbol{F}$ acting on the surface of the bisecting plane by a single star is perpendicular to it and its magnitude $F\equiv|\boldsymbol{F}|$ is obtained from the normal component of the osmotic pressure $\Pi(r)$ as

$$F(D) \approx \int_{\mathcal{S}} \Pi(r)\cos\theta \, d\mathcal{S}, \tag{23}$$

where $\mathcal{S}$ is the cross-section surface on the bisecting plane and $\cos\theta$ takes into account the projection normal to it. A simulation snapshot of two interacting PE stars is shown in Fig. 10, explicitly showing the arm retraction,

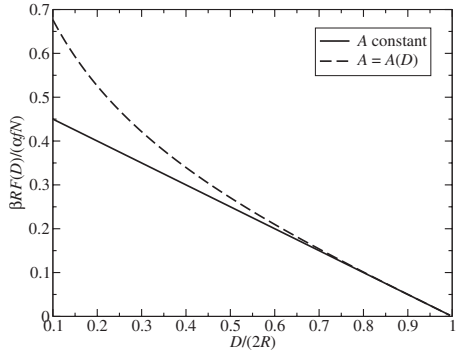

FIG. 11. The Pincus force between two stars vs distance D. Compared are the Pincus force resulting for a D-independent normalization coefficient A [Eq. (24)], solid lines, with the corrected Pincus force [Eq. (26)], dashed lines.

also referred to as "no interdigitation condition" (Pincus, 1991) and the corresponding modeling in Fig. 9. In the limit $R \gg D$, the force is given by (Pincus, 1991)

$$F(D) = kT\frac{\alpha f N(1-\tilde{D})}{2R}, \tag{24}$$

where $\tilde{D}=D/(2R)$. Pincus further uses $\tilde{D} \ll 1$ to obtain a constant force,

$$F(D) \approx kT\frac{\alpha f N}{2R}. \tag{25}$$

However, in most relevant cases D is comparable to R, and the force decays, according to Eq. (24), linearly with D. Simulations (Jusufi *et al.*, 2002a, 2002b; Wang and Denton, 2005) prove a nonlinear decay of the force, a feature not captured by Eq. (24). The above analysis neglects one important aspect, i.e., the fact that the prefactor A of the counterion density profile $c_{\text{in}}(r)=A/r^2$ depends on the distance D between the stars. In the above argument, the volume of an isolated star has been used to obtain A from Eq. (22). However, replacing Ω by a chopped sphere volume $\Omega(D)$, as sketched in Fig. 9, we obtain a distance dependent prefactor $A=A(D)$. The resulting corrected Pincus force between two stars is then given by

$$\beta RF(D) \approx \frac{\alpha f N(1-\tilde{D})}{1+\tilde{D}(1-\ln\tilde{D})}, \tag{26}$$

where $\beta=(kT)^{-1}$. Indeed, the interaction force between two stars is now a distance-dependent nonlinear function (see Fig. 11). The force is repulsive and decays monotonically with the distance. The forces expressed by Eqs. (25) and (26) all share common properties: First, the forces are repulsive and typically strong enough to stabilize PE-star solutions from precipitation. Second, the strength can be controlled through the functionality f, as for neutral stars, for which $F \sim f^{3/2}$ (Witten and Pincus, 1986). Both features are illustrated in Fig. 11. We emphasize, however, that the use of a homogeneous counterion profile results in a quantitatively erroneous force. In Sec. III.B we present a variational free-energy approach that also accounts for electrostatic effects and counterion condensation. We compare the contributions and confirm that Pincus' assumption, despite its quantitative drawbacks, is essentially and *physically* correct: the most dominant contribution for the interaction results from the entropic changes of confined counterions.

B. Variational free-energy approach

We extend the three-state cell model of a single star, as described in Sec. II.C, and apply it to the case of two interacting stars. The two-star cell model is sketched in Fig. 9, where both PE stars are represented by two fused spheres of volume $V_{\text{in}}(D)$ inside a cell consisting of two fused spherical cells of radius R_W. Beyond overlap $D>2R$ the interaction can be well described by a Yukawa-type (Debye-Hückel) potential that accounts for Coulomb screening through the remaining free counterions. Note that the effective charge of a single star is small, which leads to low surface potential energy ($<kT$), for which the Debye-Hückel approach is justified. This is in line with the theory of charged colloids (Hansen and Löwen, 2000) and has been confirmed through the application of linear response theory to PE stars (Denton, 2003) (see Sec. III.D). In what follows, therefore, we focus on the interaction for overlapping distances.

The effective interaction energy between two stars is defined as

$$V_{\text{eff}}(D) = \mathcal{F}_2(D) - \mathcal{F}_2(D \to \infty), \tag{27}$$

where $\mathcal{F}_2(D)$ is the Helmholtz free energy of two PE stars at separation D. Note that $\mathcal{F}_2(D\to\infty)=2\mathcal{F}$, i.e., the free energy of two isolated stars. In principle, the Helmholtz free energy of the system is a sum of all contributions that are listed in Eqs. (12)–(16). The distance dependence enters through the volumes $V_{\text{in}}(D)$ and $V_{\text{out}}(D)$ and needs to be considered in Eqs. (12) and (14). Some contributions drop out in Eq. (27) since they do not depend on the distance D, e.g., $\mathcal{F}_{\text{fl}}(D)=2\mathcal{F}_{\text{fl}}$. The remaining free-energy contributions are $U_{\text{H}}(D)$ and $-T\Sigma_{i=1}^{3}S_i(D)$, $i=1,2,3$. The entropic terms can be calculated analytically. We account for counterion condensation, i.e., Manning-condensed counterions around the chains still exist despite the chain retraction. For $S_2(D)$, the entropic contribution of noncondensed counterions inside the star and for $U_{\text{H}}(D)$ the $1/r^2$ decay of the density profile has been employed: $\varrho(r)\sim c_{\text{in}}(r)\sim A(D)/r^2$, where $A(D)$ has been used in Eq. (26). For the geometry sketched in Fig. 9 the electrostatic energy $U_{\text{H}}(D)$ cannot be expressed in a closed form; it takes rather the form of a series of analytical functions and it has to be solved numerically at each given distance D. Details of the calculations can be found in Jusufi *et al.* (2002b), where it was shown that the electrostatic energy $U_{\text{H}}(D)$ and the entropy of confined noncondensed counterions $S_2(D)$ exhibit the strongest D dependence. The other contributions vary modestly with D and therefore hardly contribute to the effective force $F(D)=-dV_{\text{eff}}/dD$. Note that

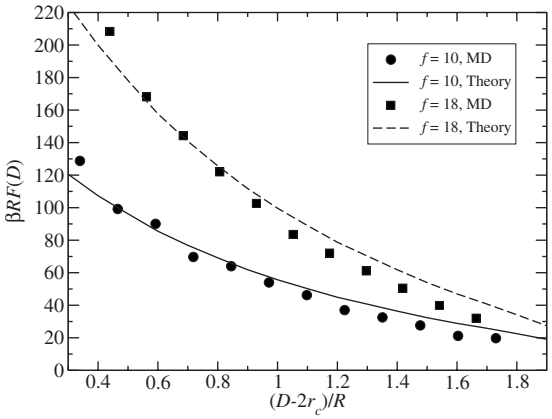

FIG. 12. Effective force $F(D)=-dV_{\rm eff}/dD$ between two PE stars versus distance D. Shown are results for 10 arm stars (solid line) and 18 arm stars (dashed line) with $\alpha=1/3$ and $N=50$. For comparison, the effective core diameter $2r_c$, which is implemented in the simulation model (results represented by symbols), needs to be subtracted (Jusufi *et al.*, 2002a, 2002b).

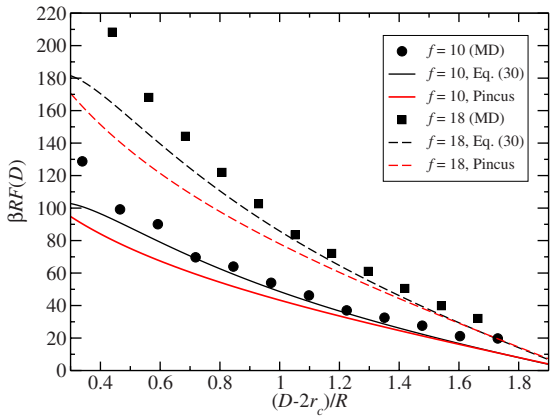

FIG. 13. (Color online) Approximated effective force $F(D)=-dV_{\rm eff}/dD$ between two stars with $V_{\rm eff}(D)$ from Eq. (30) compared with MD results (Jusufi *et al.*, 2004). Parameters are the same as in Fig. 12. Also shown is the corrected Pincus force according to Eq. (26).

the entropic contribution $S_2(D)$ scales with $N_2=N_{\rm in}-N_1$, the number of noncondensed counterions inside the stars, similar to Eq. (10). This underlines the importance of counterion condensation since N_2 sets the strength of the interaction. This feature corresponds to a renormalization of the effective entropic energy inside the star since without condensation the effective potential would be much higher.

The resulting contributions are added up and minimized with respect to R and the number of counterions in their three distinct states N_i. The effective interaction $V_{\rm eff}(D)$ is then given by

$$V_{\rm eff}(D)=\min_{\{R,\{N_i\}\}}\left\{U_{\rm H}(D)-T\sum_{i=1}^{3}S_i(D)\right\}. \tag{28}$$

In Fig. 12, the results for the effective force $F(D)=-dV_{\rm eff}/dD$ between two PE stars with different parameters are shown and compared with MD simulation results (Jusufi *et al.*, 2002a, 2002b). The agreement is good over a wide range of overlapping distances $D<2R$. Note that the simulation model possesses a microscopic core of sizes $r_c=0.04R$ and $0.05R$ for $f=10$ and 18, respectively, which need to be subtracted from the separation D for comparison reasons. The repulsion decays weakly with D. Its scale can be tuned by the parameters α and f. In fact, the repulsion is mainly governed by the entropic terms of confined counterions. In order to check the dominance of this term, we reformulate the effective interaction potential in Eq. (28) via

$$V_{\rm eff}(D)\approx -T[S_{\rm in}(D)-S_{\rm in}(D\to\infty)], \tag{29}$$

where we neglected electrostatic terms and the entropic contributions of condensed and free counterions since they do not vary much if the distance D is changed. We subtract the condensed counterions from the confined ones, i.e., $N_2=N_{\rm in}-N_1$, and assume $N_3=0$ (no counterions outside the stars). With those simplifications, the result for the effective interaction potential becomes analytical, namely,

$$V_{\rm eff}(D)\approx 2N_2\left[\ln\left(\frac{2}{K}\right)+\frac{D}{2RK}\ln^2\left(\frac{D}{2R}\right)\right], \tag{30}$$

where

$$K(D)=1+\frac{D}{2R}\left[1-\ln\left(\frac{D}{2R}\right)\right]. \tag{31}$$

An analogous form has been reported for PE brushes with a finite colloidal core radius in Jusufi *et al.* (2004). Note that $N_2=\alpha fN-N_1$ since there are no free counterions in this approximation.

For simplicity, we estimate $N_1=(1-1/\alpha u^2)\alpha fN$, yielding $N_2=53$ for the 10 arm star and $N_2=96$ for the 18 arm star, for which force results are shown in Fig. 13. The agreement with MD results is again reasonable over a wide distance region D despite the simplifications made. Only at strong overlap the discrepancies become larger. The maximum of the entropic terms at small distances arises from the $1/r^2$ increase of the local counterion density as $r\to 0$. In reality, the density at the inner core is finite and steric repulsions would increase the entropic term further as $D\to 0$. In the same figure we also show results from the corrected Pincus force, which is also analytically available [Eq. (26)]. At large separations, the force agrees well with simulation results but it underestimates the same at the small separation regime $D\lesssim R$. Note that in the Pincus force the complete number of ions contribute to the force, which is physically correct: even Manning-condensed counterions can freely move *along* the axial direction of the rodlike PE arms and thus do contribute to the osmotic pressure exerted on the bisecting plane, in agreement with Pincus' approach. For this case, then, no further "renormalization" due to the condensed counterions is necessary.

The agreement of both the approximated effective potential from Eq. (30) and Pincus' results with MD calculations demonstrates the dominant role of the counter-

ion entropy for the effective interaction potential, as already recognized by Pincus (1991). Electrostatic effects are of minor importance since the strong counterion absorption in the star interior renders the stars quasi-neutral. The degree of neutralization is, of course, concentration dependent and above the stars' overlap density in a concentrated solution these are fully electrically neutral. Condensation is relevant for setting the scale of the potential, whereas the $1/r^2$ decay in the counterion density and the retraction of the chains lead to a nonlinear decay of the force. Note that the approximate expression [Eq. (30)], applied on spherical polyelectrolyte brushes with a finite core (Jusufi *et al.*, 2004) has been recently confirmed by direct force measurements, including salted solutions of PE-brush systems (Dominguez-Espinosa *et al.*, 2008; Huang *et al.*, 2009).

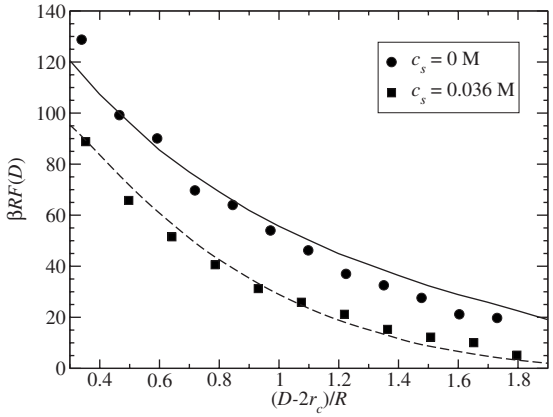

FIG. 14. Effective force $F=-dV_{\mathrm{eff}}/dD$ between two stars with and without added salt, lines, as compared with MD results, symbols (Jusufi *et al.*, 2004). Star parameters: $\alpha=1/3$, $f=10$, $N=50$. From Jusufi *et al.*, 2002b.

C. Effects of salt

In Sec. II.D it was shown that added salt induces a shrinkage of a single star in particular if the salt concentration exceeds the counterion concentration inside the star. The shrinkage was attributed to the salt-dependent osmotic pressure balance of the ions inside and outside the stars. Within the variational free-energy approach, the entropic term S_3 changes significantly now since one needs to replace the number of free ions $N_3=\alpha fN-N_{\mathrm{in}} \rightarrow \alpha fN+2N_s-N_{\mathrm{in}}$, with N_s the number of salt ion pairs. For the effective interaction [Eq. (28)], the D dependence of $S_3(D)$ becomes important as well due to $V_{\mathrm{out}}(D)$. The analytical expression [Eq. (30)] is no longer valid unless the star density is very dilute, i.e., $V_{\mathrm{out}} \gg V_{\mathrm{in}}$. In such cases, changes in the entropy of ions in the outer volume are negligible and the approximate solution [Eq. (30)] still holds, as was recently confirmed by direct force measurements (Dominguez-Espinosa *et al.*, 2008).

In general, however, when $V_{\mathrm{out}} > V_{\mathrm{in}}$ (both volumes are in the same order of magnitude), the change of the outer volume $V_{\mathrm{out}}(D)$ is crucial since it grows as the star distance D decreases (see Fig. 9). Accounting for these changes in the full variational free-energy approach, we obtain the effective interaction force between two stars in the presence of added salt. In Fig. 14, the salt effect is demonstrated for two ten arm stars with and without added salt (Jusufi *et al.*, 2002b). The repulsion becomes weaker when salt is present. The mechanism is similar to depletion effects (Likos, 2001) known from classical case of colloid-polymer mixture (Dijkstra, Brader, and Evans, 1999). The two overlapping stars are "hit" by the enhanced number of ions outside the stars, which induce an attractive depletion force. This attraction is, however, overbalanced by the strong repulsive forces stemming form the confined ions since the stars are penetrable. The net force is a reduced repulsion compared to the salt-free case, as shown in Fig. 14, already for a modest salt concentration of $c_s=0.036M$.

A different approach to the calculation of the effective forces was given by Wang and Denton (2005). Here, instead of dealing with the bare Coulomb interactions of the charged monomers, the counterions, and possible coions (in the case of added salt), one resorts to the employment of a screened-Coulomb (Yukawa) interaction between the charged monomers of the chains from the outset. In particular, Wang and Denton modeled the PE-star arms as rigid freely rotating rods anchored on a common central point and consisting of N_b beads, each interacting with the other via a Yukawa potential. The bead-bead separation is denoted a (monomer size), and the orientation of the arm is given by the unit vector $\hat{\boldsymbol{u}}$, as sketched in Fig. 15. In this approach, the screened electrostatic interaction between any two arms, oriented along $\hat{\boldsymbol{u}}$ and $\hat{\boldsymbol{u}}'$ and anchored in two stars separated by the vector $\boldsymbol{D}$, is expressed as

$$v_{\mathrm{arm}}(\hat{\boldsymbol{u}},\hat{\boldsymbol{u}}';\boldsymbol{D}) = \frac{z^2e^2}{\epsilon}\sum_{i=1}^{N_b}\sum_{j=1}^{N_b}\frac{\exp(-\kappa|\boldsymbol{D}+ia\hat{\boldsymbol{u}}-ja\hat{\boldsymbol{u}}'|)}{|\boldsymbol{D}+ia\hat{\boldsymbol{u}}-ja\hat{\boldsymbol{u}}'|}, \tag{32}$$

where z is the valency of each bead (charged monomer) and $\kappa=\sqrt{4\pi e^2(z^2fN_b\rho+2q^2c_s)/\epsilon kT}$ is the inverse Debye screening length in a PE-star solution of density ρ, con-

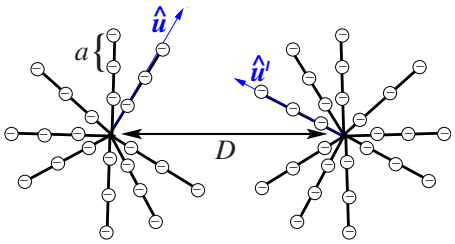

FIG. 15. (Color online) Sketch of the Wang-Denton model for two interacting PE stars. Each arm is modeled as a rigid freely rotating rod, on which monomers are located in regular separations a from each other. The monomer-monomer interaction is modeled by a Yukawa potential to take into account the screening by counterions and salt [see Eq. (32)]. From Wang and Denton, 2005.

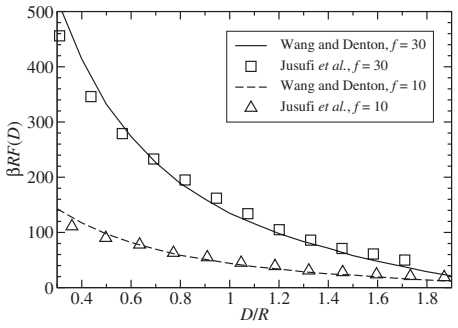

FIG. 16. Comparison of forces $F(D)$ between two PE stars of radius R as a function of their center-to-center separation D from the Yukawa-segment MC simulations of Wang and Denton (2005) and the fully microscopic Coulomb MD simulations of Jusufi *et al.* (2002b). Courtesy of A. R. Denton.

taining in addition a concentration c_s of q-valent salt counter and coions. They performed Monte Carlo (MC) simulations supplemented by density-functional theory (DFT) calculations for the effective force $F(D)$ between the PE-star centers. In the former, they fully confirmed the picture of arm retraction (no interdigitation) upon approach of the stars, which was explicitly implemented in the DFT calculations as well. The resulting effective force from the MC simulations is in good agreement with the MD results of Jusufi *et al.* (2002a, 2002b), as shown in Fig. 16. We note that Wang and Denton had to renormalize the bare charge $Q_b e$ of the PE stars by taking into account the Manning-condensed counterions, which do not contribute to screening; it is rewarding that the numbers N_1 of condensed counterions employed in Wang and Denton (2005) are in close agreement with the ones found by the free-energy minimization approach in Jusufi *et al.* (2002b). These features demonstrate independently both the validity of the modeling of the interacting PE stars and the insensitivity of the physics on the level of description of the electrostatic interactions: fully microscopic (Jusufi *et al.*, 2002b) versus effectively screened from the counterions and salt (Wang and Denton, 2005).

A final note should be made on the case of multivalent salt ions. We showed in Sec. II.D that multivalent ions dramatically alter the conformation of the star, i.e., they induce a collapse. The resulting star is a globular object with a mixture of monomers and multivalent ions strongly correlated with each other. In experiments, coagulation effects are observed at minute concentrations (Mei *et al.*, 2008). This coagulation is caused by short-ranged attractions between stars (Schneider *et al.*, 2008), which are attributed to ion-bridging effects. There are also ongoing discussions about charge reversal of the stars due to condensed multivalent counterions (Grosberg *et al.*, 2002), which might play a further role for the interactions. These correlation effects are difficult to employ in a variational free-energy approach and it remains an open task for quantifying those effects within a suitable theoretical framework.

D. Linear response theory

An alternative approach to the theory of effective PE-star interactions has been developed by Denton (2003). This approach also yields simultaneously information on single star characteristics (e.g., counterion adsorption and profiles) as well as on interactions. Since there are close connections with the variational free-energy approach presented in Secs. II.C and III.B, we discuss the main points of Denton's approach here, referring the interested reader to Denton (2003), for details.

We have seen that electrostatic effects are negligible for interacting stars within overlapping distances. It was shown that the entropic terms of confined counterions predominantly determine the repulsive force between the stars. These effects can also be discussed in an approach that starts with a given charge distribution in the interior of a macroion [$\rho(r) \sim 1/r^2$ in the PE-star case] and considers the *response* of the counterion cloud to it. This is inspired from similar approaches to charged *hard* colloids (Hansen and Löwen, 2000) but in contrast to the latter, PE stars are *penetrable*: the counterions can wander in their interior. Accordingly, the PE stars are modeled as penetrable macroions in the presence of counterions in solution. The specific character of a PE star enters through the conformational property of macroions, defined below. The mixture of macroions and counterions is treated by taking a one-component plasma as a reference state, in which the macroions are seen as an external perturbation. To account for the reaction of the counterions on this field, linear response theory (LRT) is employed. Within the LRT framework, the response of the counterions to the external field is expressed through a linear relationship between the Fourier transforms of the counterion distribution $c(r)$ and the macroion-counterion interaction $V_{mc}(r)$ at separation r, namely,

$$\hat{c}(k) = \chi(k)\hat{V}_{mc}(k)\hat{\rho}(k), \tag{33}$$

with $\hat{c}(k)$ and $\hat{\rho}(k)$ being the Fourier transforms of the counterion and monomer density distributions $c(r)$ and $\rho(r)$, respectively. Further, $\hat{V}_{mc}(k)$ is the Fourier transform of $V_{mc}(r)$, where k is the wave number. For weakly coupled ion systems, the linear response function $\chi(k)$ is expressed as (Canessa *et al.*, 1988; Grimson and Silbert, 1991; Denton, 1999, 2000)

$$\chi(k) = -\frac{n_c}{kT(1+\kappa^2/k^2)}, \tag{34}$$

with $\kappa = \sqrt{4\pi n_c q^2 \lambda_B}$ the inverse Debye screening length and n_c the counterion number density; in the presence of salt, one replaces $n_c \to n_c + 2c_s$, with c_s the number density of salt ion pairs. Notice that by virtue of Eqs. (33) and (34), one can immediately calculate the response profile $c(r)$ of the counterions to a macroion fixed at the origin for a given macroion-counterion (electrostatic) interaction potential $V_{mc}(r)$. Accordingly, the fraction of counterions f_{in} adsorbed within the PE star can also be evaluated analytically within the LRT and is expressed

as $4\pi\int_0^R r^2 c(r)dr$ divided by the total counterion number released by a single star. For the potential $V_{mc}(r)$ corresponding to PE stars, the result is given by (Denton, 2003)

$$f_{\text{in}} = 1 - \left(1 + \frac{1}{\kappa R}\right)\exp(-\kappa R)\text{sinhc}(\kappa R), \tag{35}$$

where

$$\text{sinhc}(x) \equiv \int_0^x du \frac{\sinh(u)}{u} = \sum_{n=0}^{\infty} \frac{x^{2n+1}}{(2n+1)(2n+1)!}. \tag{36}$$

The result of Eq. (35) is in agreement with the findings in Sec. II.C (variational free-energy approach), confirming the strong absorption of counterions in the star interior as the star concentration grows. In particular, $f_{\text{in}} \to 0$ as $\kappa R \to 0$ and $f_{\text{in}} \to 1$ as $\kappa R \to \infty$.

Within LRT, the effective interaction between two macroions at separation D is expressed as the sum of the bare macroion-macroion contribution $V_{mm}(D)$ and the counterion-induced interaction $V_{\text{ind}}(D)$, namely,

$$V_{\text{eff}}(D) = V_{mm}(D) + V_{\text{ind}}(D). \tag{37}$$

This expression emphasizes the meaning of $V_{\text{eff}}(D)$ as a "dressed" or renormalized interaction between the PE stars caused by the presence of the mobile counterions. The form of $V_{mm}(D)$ depends on the macroion conformation. Denton assumed, for simplicity, that it can be given as an "overlap integral" between the undisturbed macroion (charge) densities, weighted with the Coulomb-interaction kernel, i.e., the no-interdigitation condition and the chain retraction are ignored at this level of description and the result is given by (Denton, 2003)

$$V_{mm}(D) = \frac{e^2}{\epsilon}\int d^3r \int d^3r' \frac{\rho(\boldsymbol{r})\rho(\boldsymbol{r}')}{|\boldsymbol{r} - \boldsymbol{r}' - \boldsymbol{D}|}. \tag{38}$$

In Eq. (38) a key ingredient is the r dependence of $\rho(r)$, for which the form $\rho(r) = fN/4\pi R r^2$ has been chosen. Similarly to the variational free-energy approach, therefore, the physical picture of stretched arms has been adopted. By virtue of Gauss' law, $V_{mm}(D)$ reduces to the bare Coulomb interaction $V_{mm}(D) = (Q_b e)^2/(\epsilon D)$ for $D > 2R$ (spherically symmetric macroions), where Q_b is the PE-star valency. The solution of Eq. (38) for $D \leqslant 2R$ can again be expressed in closed form, but it is lengthy; it features two different mathematical expressions, one for $D \leqslant R$ and one for $R < D \leqslant 2R$, and can be found in the Appendix of Denton (2003).

The counterion-induced interaction $V_{\text{ind}}(D)$ takes a particularly simple form in Fourier space, namely,

$$\hat{V}_{\text{ind}}(k) = \chi(k)[\hat{V}_{mc}(k)]^2. \tag{39}$$

Therefore, the key remaining quantity is the (bare) electrostatic interaction potential $V_{mc}(r)$ acting between a macroion held fixed at the origin and a microion at a distance r from its center. For the determination of $V_{mc}(r)$, we begin with the radial electric field $E(r)$ of a star-branched macroion using the $1/r^2$ dependence of the charge density and Gauss' law to obtain

$$E(r) = \begin{cases} -\dfrac{Q_b q}{\epsilon R r}, & r \leqslant R \\ -\dfrac{Q_b q}{\epsilon r^2}, & r > R. \end{cases} \tag{40}$$

Equation (40) readily yields the electrostatic potential energy $V_{mc}(r)$ through integration over r as

$$V_{mc}(r) = \begin{cases} -\dfrac{Q_b q}{\epsilon R}\left[1 - \ln\left(\dfrac{r}{R}\right)\right], & r \leqslant R \\ -\dfrac{Q_b q}{\epsilon r}, & r > R. \end{cases} \tag{41}$$

Using the Fourier transform of Eqs. (41) and (34), we obtain $\hat{V}_{\text{ind}}(k)$ [Eq. (39)] from which via an inverse Fourier transform $V_{\text{ind}}(D)$ can be gained in the form

$$V_{\text{ind}}(D) = -\frac{(4\pi Q_b \kappa R)^2}{\epsilon D}\int_0^{\infty} dx \frac{\sin(xD/R)}{x^3(x^2 + \kappa^2 R^2)}\text{sinc}^2 x, \tag{42}$$

with $\text{sinc}(x) \equiv \int_0^x du\, \sin(u)/u$.

The effective potential $V_{\text{eff}}(D)$ is now obtained from Eq. (37) and the results for $V_{mm}(D)$ and $V_{\text{ind}}(D)$ summarized above. For nonoverlapping stars ($D > 2R$), $V_{\text{eff}}(D)$ has a simple analytical form

$$V_{\text{eff}}(D) = \frac{Q_b^2}{\epsilon}\left[\frac{\text{sinhc}(\kappa R)}{\kappa R}\right]^2 \frac{\exp(-\kappa D)}{D}, \quad D > 2R. \tag{43}$$

The result of Eq. (43) is indeed a Yukawa screening electrostatic potential of the same form as that for charged colloidal suspensions, albeit with a different prefactor, reflecting the penetrability of the stars. In this way, the anticipations in the beginning of Sec. III.B are confirmed. For overlapping distances $D \leqslant 2R$, $V_{\text{eff}}(D)$ cannot be cast in a closed form. However, the numerical result shown in Fig. 17 confirms the qualitative similarity with the results of the variational-approach method: in

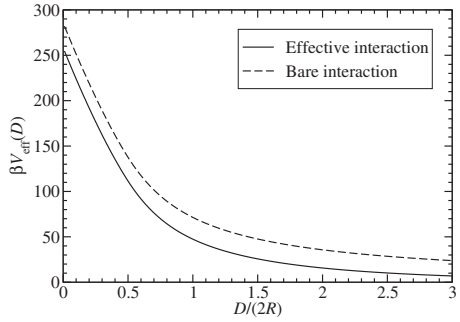

FIG. 17. The LRT result for the effective interaction potential between two PE stars of diameter $2R = 100$ nm and bare charge $Q_b = 100$ (Denton, 2003). The results pertain to a system with packing fraction $\pi\rho\sigma^3/6 = 0.01$ at room temperature, $\lambda_B = 0.71$ nm. Courtesy of A. R. Denton.

both cases, a soft, penetrable, and nondiverging interaction is obtained for overlapping distances, smoothly crossing over to a Yukawa repulsion for nonoverlapping ones.

The LRT approach has also been generalized to spherical polyelectrolyte brushes (SPBs) possessing a finite core by Wang and Denton (2004). The modification made with respect to PE stars was to introduce an impenetrable core region, $r<b$, within which $\rho(r)=c(r)=0$, leaving $\rho(r)\sim 1/r^2$ unchanged for $b\leqslant r<R$, where R is the overall brush radius. It was shown in a systematic way that SPBs interpolate between stars ($b\to 0$) and charge-stabilized hard colloids ($b\to R$) regarding all aspects: counterion penetration, counterion profiles, and effective interactions. These facts bring about an important advantage of the LRT approach, namely, that with a change in the functional form of the macroion internal density distribution $\rho(r)$, it can be readily applied to any penetrable polyelectrolyte-based macromolecule. In this spirit, Denton also applied LRT to loosely cross-linked ionic microgels, for which a homogeneous profile, $\rho(r)=(3Q/4\pi R^3)\Theta(R-r)$, has been assumed. For this case, the effective interaction $V_{\rm eff}(D)$ obtained can even be cast in a closed form (Denton, 2003), which is similar to the one for PE stars. This results in concomitant similarities in the phase behavior of the two systems, discussed in the following section.

IV. THE MANY-BODY SYSTEM: CORRELATIONS AND PHASE BEHAVIOR

The effective interaction potential $V_{\rm eff}(D)$ allows now for the next step in the coarse-graining procedure: a concentrated solution of PE stars can be considered as a collection of "point particles" (the PE-star centers) that interact via $V_{\rm eff}(D)$. Accordingly, a complex fluid has been effectively reduced to a simple one and the standard procedures for calculating structure and thermodynamics (Hansen and McDonald, 2005) can also be employed to this system. This should be done with care, nevertheless, because there are some caveats involved, which have to do with the procedure of coarse graining that leads to the derivation of the effective interaction potential $V_{\rm eff}(D)$. These have to do with the density dependence of the latter, with the unavoidable presence of many-body forces and with the appearance of volume terms in the system's Hamiltonian. We discuss these below.

In Fig. 18 we show typical shapes of the effective interaction $V_{\rm eff}(D)$, obtained by the variational free-energy method outlined in Sec. III.B for different values of the PE-star density ρ, while T is kept fixed at room temperature. The effective potential is *density dependent* as long as ρ lies below its overlap value ρ^*, the latter defined via $(\pi/6)\rho^*\sigma^3=1$. The origin of this density dependence lies in the existence of free interstar space for $\rho<\rho^*$, which allows the counterions to adjust their population between the adsorbed and free states according to ρ and, thus, the available free volume parametrized by

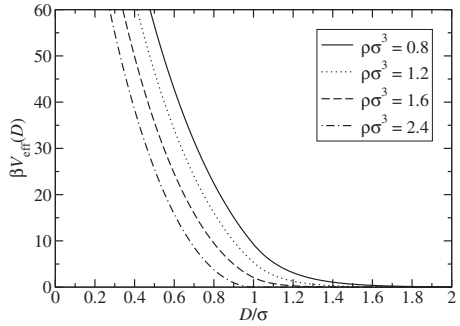

FIG. 18. The effective interaction potential between PE stars with $f=15$ arms and degree of charging $\alpha=1/3$ as a function of center-to-center separation D scaled over the star diameter σ. Results are shown for four different values of the star density $\rho\sigma^3$ as indicated in the legend. From Hoffmann *et al.*, 2004.

the radius of the Wigner-Seitz cell (see Secs. II.C and III.B). This has a double effect: on the one hand, it influences the screening length κ, which enters the Yukawa form of the interaction $V_{\rm eff}(D)$ for $D>\sigma$ and, on the other hand, it affects the number of adsorbed counterions that sets the scale of the same for $D\leqslant\sigma$. At the overlap density $R_W=R$ the free volume disappears and, from then on, all counterions are adsorbed. Hence, $V_{\rm eff}(D)$ becomes density independent. For more details on the form of $V_{\rm eff}(D)$ and the "matching" of its forms for $D\leqslant\sigma$ and $D>\sigma$, see Hoffmann *et al.* (2004). Apart from the density dependence, the interaction is also soft, corresponding to the penetrable character of the PE stars.

On the basis of $V_{\rm eff}(D)$, typical pair correlation functions of the fluid, such as the radial distribution function $g(r)$ or its Fourier-space analog, the structure factor $S(k)=1+\rho\int d^3r\,\exp[-i\boldsymbol{k}\cdot\boldsymbol{r}]h(r)$, where $h(r)=g(r)-1$, can be calculated by, e.g., liquid integral equation theories. Representative results from Hoffmann *et al.* (2004), obtained by closing the Ornstein-Zernike relation (Hansen and McDonald, 2005) with the Rogers-Young closure (Rogers and Young, 1984), are shown in Fig. 19. A first feature that can be discerned there is that the height of the maximum of $S(k)$ never exceeds the Hansen-Verlet value of 2.85, which sets an empirical threshold for the

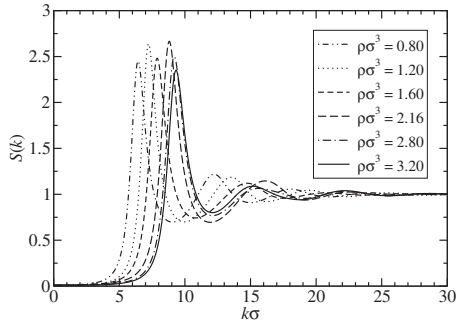

FIG. 19. The structure factor of concentrated PE-star solutions for different star densities $\rho\sigma^3$ as indicated in the legend. As in Fig. 18, the results pertain to stars with $f=15$ arms and charge fraction $\alpha=1/3$. From Hoffmann *et al.*, 2004.

onset of crystallization (Hansen and Verlet, 1969). Indeed, as confirmed by free-energy calculations, the soft repulsion between PE stars with $f=15$ and $\alpha=1/3$ is too weak to support crystallization, so that the system remains fluid at all concentrations (Hoffmann *et al.*, 2004). Further, above the overlap density, the wave number k_* at which the maximum occurs does not scale anymore with the power law $k_* \sim \rho^{1/3}$ but it becomes rather insensitive to the density. This feature has been experimentally observed in small-angle x-ray scattering experiments from concentrated solutions of star-branched polyelectrolytes in particular in ten arm poly(styrene-co-sodium styrene sulphonate) systems (Heinrich *et al.*, 2001). In addition, the height of the maximum starts decreasing with ρ. All these characteristics are signatures of the soft nature of the repulsion and have also been observed in the cases of two related systems: neutral star polymers (Likos *et al.*, 1998; Watzlawek *et al.*, 1998) as well as ionic microgels (Gottwald *et al.*, 2004, 2005) show similar behavior in the density dependence of their pair correlation functions.

The calculation of the phase diagram requires the evaluation of the (Helmholtz) free energies of candidate phases and the comparison among those. Here one has to be careful how to carry out this task since $V_{\mathrm{eff}}(D)$ is an *effective* and not a *microscopic* potential; stated differently, $V_{\mathrm{eff}}(D)$ is *itself* a partial Helmholtz free energy [see Eq. (27)]. As pointed out (Louis, 2002), effective interaction potentials have to be used in the context of the procedure in which they have been derived when one aims at calculating thermodynamic quantities on their basis. Whereas various thermodynamics routes (energy, pressure, compressibility, etc.) to the free energy should all lead to the same result when microscopic state-independent interactions are employed, this is not the case for effective state-dependent potentials. Hoffmann *et al.* (2004) demonstrated that for the way in which $V_{\mathrm{eff}}(D)$ of PE stars has been derived, the correct way to proceed with the thermodynamics of the fluid system is based on the functional relationship (Evans, 1979)

$$\frac{\delta \mathcal{F}_{\mathrm{ex}}[V_{\mathrm{eff}}]}{\delta V_{\mathrm{eff}}(|\boldsymbol{r}-\boldsymbol{r}'|)} = \frac{1}{2}\rho^2 g(|\boldsymbol{r}-\boldsymbol{r}'|), \tag{44}$$

in which the excess Helmholtz free energy of the system $\mathcal{F}_{\mathrm{ex}}$ is viewed as a functional of $V_{\mathrm{eff}}(D)$. This relationship then leads to the so-called λ-integration route to the excess free energy per volume $f_{\mathrm{ex}}(\rho)$. Here one introduces a scaled version of the effective interaction $V_{\mathrm{eff}}^{(\lambda)}(D) \equiv \lambda V_{\mathrm{eff}}(D)$ at fixed density ρ, where $0 \leqslant \lambda \leqslant 1$. For each λ value, the corresponding radial distribution function $g^{(\lambda)}(D)$ is calculated and $f_{\mathrm{ex}}(\rho)$ is expressed as (Hoffmann *et al.*, 2004)

$$f_{\mathrm{ex}}(\rho) = \frac{1}{2}\rho^2 \int d^3D V_{\mathrm{eff}}(D) \int_0^1 d\lambda g^{(\lambda)}(D). \tag{45}$$

To obtain the full free-energy density $f_{\mathrm{fl}}(\rho)$ of the fluid state, the ideal term $f_{\mathrm{id}}(\rho)=k_B T\rho[\ln(\rho\sigma^3)-1]$ as well as a volume term $f_{\mathrm{vol}}(\rho)$ has to be added to $f_{\mathrm{ex}}(\rho)$ above. Whereas the former arises, evidently, from the integration of the PE-star momenta in the partition function of the system, the latter has its origin at the integrated-out counterion degrees of freedom. Accordingly, it includes not only the counterions' kinetic contributions to the free energy but also those from their binding to the macroions. Volume terms obtain their name from the fact that they arise from a configuration-independent term in the effective Hamiltonian and they have, therefore, no effect on the correlation functions of the PE stars but they do influence the thermodynamics. Their existence is ubiquitous in charged systems, in particular, both in the classical (van Roij *et al.*, 1999; Harreis *et al.*, 2002, 2003) and in the quantal (Ashcroft and Stroud, 1987) regimes. Since the process leading to $V_{\mathrm{eff}}(D)$ for PE stars has been one that commences at the microscopic level, one can keep track of the volume term, which turns out to be given by $f_{\mathrm{vol}}(\rho)=\rho f_1(\rho)$; here $f_1(\rho)$ is the free energy of a *single* star and its dependence on ρ comes through the freedom of counterions to partition themselves between its interior and its exterior. Similarly to $V_{\mathrm{eff}}(D)$, the density dependence of $f_1(\rho)$ disappears for $\rho \geqslant \rho^*$ and the volume term becomes an irrelevant linear function of the density that does not affect possible phase boundaries.

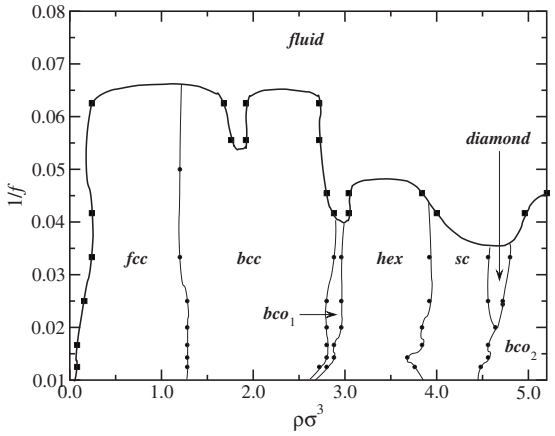

FIG. 20. The phase diagram of PE stars with charge fraction $\alpha=1/3$ plotted on the inverse functionality vs density representation. Phase boundaries between coexisting phases are calculated at the discrete f values indicated by the points. The width of the two-phase coexistence regions is negligible on the scale shown, whereas all lines are guides for the eye connecting the calculated phase boundaries at the points shown. From Hoffmann *et al.*, 2004.

The Helmholtz free energy of the fluid is then compared with that of several candidate solid phases $f_{\mathrm{sol}}(\rho)$. Hoffmann *et al.* obtained the latter by employing an approximate Einstein model for the crystals, supplementing of course the free energies of the latter with the volume terms (Hoffmann *et al.*, 2004). The resulting phase diagram is shown in Fig. 20. The diagram displays the features that are characteristic for ultrasoft interaction potentials: absence of freezing below a minimum functionality f_{min}, as well as the stability of a multitude

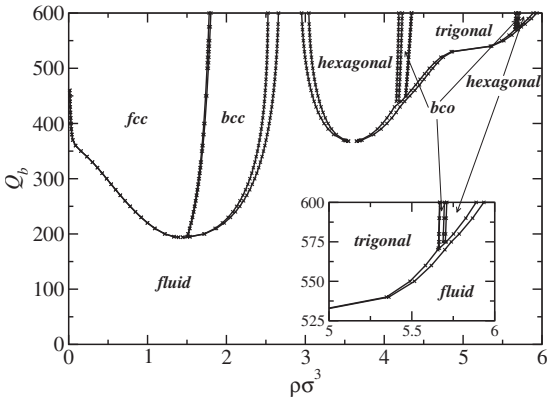

FIG. 21. The phase diagram of ionic microgels, plotted in the bare charge vs density representation (Gottwald *et al.*, 2004, 2005). Note that the quantity Q_b on the vertical axis plays for microgels a role analogous to f for PE stars. The phase diagram here thus has a topology similar to that of Fig. 20 if looked "upside down."

of exotic structures at high concentrations, although the interaction is a simple spherically symmetric one. Some powerful and elegant geometric arguments for the latter characteristic have been suggested by Ziherl and Kamien (2000, 2001), making an analogy between soft particles and soap froths. All of these features have also been seen in the phase diagrams of other similar soft systems, such as neutral star polymers (Watzlawek *et al.*, 1999) and ionic microgels (Gottwald *et al.*, 2004, 2005). The simplest model in which re-entrant melting, accompanied by a maximum freezing temperature $T_{\max}$ (the analog of the minimum freezing functionality $f_{\min}$ for stars), is the Gaussian core model of Stillinger (1976) (Lang *et al.*, 2000).

Self-organization of poly(acrylic acid) PE stars with $f=30$ and 97 arms into bcc crystals at the overlap concentration has been experimentally seen in the SAXS study of Furukawa and Ishizu (2005), in agreement with the theoretical predictions in Fig. 20. The occurrence of fcc crystals at lower densities predicted by Hoffmann *et al.* (2004) has not been reported however. On the other hand, recent experimental work by Mohanty and Richtering (2008) on ionic microgels confirmed the sequence of transitions: fluid→fcc→bcc→amorphous with increasing concentration ρ shown in Fig. 21. The last in this cascade of phases is an amorphous *glassy* state in the experiment, whereas an ergodic fluid is predicted by theory; it remains to be seen whether this glass could be, in fact, a very viscous fluid or a metastable state with some other crystal as the true equilibrium.

Finally, we discuss the magnitude and effects of many-body forces, i.e., terms in the potential energy of the effective Hamiltonian that depend on n-particle coordinates, $n \geqslant 3$, which are ubiquitous as a result of the coarse-graining procedure (Dijkstra, van Roij, and Evans, 1999). At concentrations considerably higher than ρ^*, higher-order effective interactions that go beyond the pair potential approximation begin, of course, to also play a role. For PE stars, which interact mainly through the mechanism of mutual reduction of the volume in their interior available to counterions, one expects that the strength of n-body forces will scale roughly with the volume of regions in which n spheres of radius R mutually overlap. These contributions are density and geometry dependent and thus require much more effort in being parametrized than pair interactions. For hard colloids, silica particle with diameter of 990 nm carrying a few thousand elementary charges, the $n=3$ body forces have been measured with optical tweezers and analyzed theoretically via Poisson-Boltzmann theory (Brunner *et al.*, 2004; Dobnikar *et al.*, 2004). It was found that when three particles are arranged in an isosceles triangle configuration, the three-body potential is comparable to the pair interaction for typical triangle sizes of a few nanometers and *attractive* in nature. On the other hand, if two of the particles are farther than ~ 5 μm apart, three-body forces can be neglected. The mechanism leading to many-body forces for PE stars is the same as that for hard colloids, i.e., the rearrangement of the counterion cloud, with the important difference that counterions penetrate inside the stars. An estimate can be made, leading to the result that n-body forces scale roughly- as the n-body volume overlaps between penetrable spheres at a given density ρ. In this sense, preliminary calculations show that two-body potentials are still dominant for concentrations up to $\rho \cong 2\rho^*$, similar to the case of neutral star polymers (von Ferber *et al.*, 2000).

V. CONCLUSIONS AND OUTLOOK

We have presented a review of recent work on star-shaped polyelectrolytes, with emphasis on the process of coarse graining, which allows a full bridging of the gap from the microscopic to the macroscopic length scales. For osmotic PE stars, which feature strong stretching of their arms and adsorb the majority of the counterions within their coronae, the osmostic pressure of these counterions is the key quantity that determines both their sizes and their effective interactions. Charged star polymers combine in their physics aspects of star polymers (softness, penetrability, and hybrid character between chains and hard spheres) and charged colloids (mobile counterion clouds, Yukawa screening at large separations, and dependence of properties on added salt). For salt-free cases, PE stars are quasineutral due to the strong adsorption of the counterions in their interior.

At the microscopic level, PE stars are quite different than their neutral counterparts due to the presence of charged monomers along their backbones. Nevertheless, the effective interaction between PE stars has some striking similarities with that of the neutral ones in the sense that they are both *soft* and *entropic* in origin; concomitantly, one obtains also similar mesoscopic correlations and macroscopic phase behavior for both systems. For neutral athermal star polymers, it is the entropy of the self-avoiding chains that leads to an effective repulsion whereas for charged ones it is the entropy of the

trapped counterions. Furthermore, other penetrable polymer-based colloids, such as microgels and dendrimers, also show similarities to star-shaped systems, the origin of which can be traced in the ultrasoft character of the effective interaction. This allows us to consider this large variety of systems as members of a novel family of ultrasoft colloids, which indeed have attracted considerable attention in the literature in the last decade.

Notwithstanding these similarities, the microscopic differences between the soft systems can express themselves strongly when suitable external fields that couple to the relevant degrees of freedom are introduced. Athermal star polymers, for instance, do not adsorb on flat hard surfaces since they experience a fully repulsive interaction with the walls. As all charged systems, however, PE stars respond strongly to external electric fields. In fact, by applying sufficiently strong (but still throughout realistic) electric fields, one can separate the PE star from its own counterions and bring about various types of adsorption of PE stars on oppositely charged walls (Konieczny and Likos, 2007). The complexation of PE stars with oppositely charged spherical colloids is another topic of current interest, where one can tune the relative charges and sizes of the colloid and the star to bring about supercomplexes that can serve as novel patchy colloids (Likos *et al.*, 2008). Finally, recent progresses in constructing DNA- or viral-based sparse polyelectrolyte brushes with stiff or semiflexible arms (Kegler *et al.*, 2007, 2008; Huang *et al.*, 2009) seems to be another direction of interest since little is known about the properties and interaction of these novel colloidal particles in the nanometer to micrometer domains.

ACKNOWLEDGMENTS

The authors wish to thank Professor Alan R. Denton for providing figures and for fruitful discussions. This work has been supported by the Deutsche Forschungsgemenischaft (DFG). A.J. gratefully acknowledges financial support by the DFG through a Research Fellowship. C.N.L. thanks Professor Randall D. Kamien and the Department of Physics, University of Pennsylvania, where parts of this work have been carried out, for their hospitality.

REFERENCES

Alexander, S., 1977, J. Phys. (Paris) **38**, 983.
Ashcroft, N. W., and D. Stroud, 1987, Solid State Phys. **33**, 1.
Ballauff, M., 2007, Prog. Polym. Sci. **32**, 1135.
Borisov, O. V., 1996, J. Phys. II **6**, 1.
Borisov, O. V., T. M. Birshtein, and E. B. Zhulina, 1991, J. Phys. II **1**, 521.
Borisov, O. V., and E. B. Zhulina, 1997, J. Phys. II **7**, 449.
Borisov, O. V., and E. B. Zhulina, 1998, Eur. Phys. J. B **4**, 205.
Brunner, M., J. Dobnikar, H. H. von Grünberg, and C. Bechinger, 2004, Phys. Rev. Lett. **92**, 078301.
Canessa, E., M. J. Grimson, and M. Silbert, 1988, Mol. Phys. **64**, 1195.
Daoud, M., and J. P. Cotton, 1982, J. Phys. (Paris) **43**, 531.
de Gennes, P. G., 1979, *Scaling Concepts in Polymer Physics* (Cornell University Press, Ithaca).
de Gennes, P. G., 1987, Adv. Colloid Interface Sci. **27**, 189.
Denton, A. R., 1999, J. Phys.: Condens. Matter **11**, 10061.
Denton, A. R., 2000, Phys. Rev. E **62**, 3855.
Denton, A. R., 2003, Phys. Rev. E **67**, 011804.
Dijkstra, M., J. M. Brader, and R. Evans, 1999, J. Phys.: Condens. Matter **11**, 10079.
Dijkstra, M., R. van Roij, and R. Evans, 1999, Phys. Rev. E **59**, 5744.
Dingenouts, N., M. Ballauff, D. Pontoni, and T. Narayan, 2004, Macromolecules **37**, 8152.
Dobnikar, J., M. Brunner, H. H. von Grünberg, and C. Bechinger, 2004, Phys. Rev. E **69**, 031402.
Dominguez-Espinosa, G., A. Synytska, M. Drechsler, C. Gutsche, K. Kegler, P. Uhlmann, M. Stamm, and F. Kremer, 2008, Polymer **49**, 4802.
Evans, R., 1979, Adv. Phys. **28**, 143.
Flory, P. J., 1953, *Principles of Polymer Chemistry* (Cornell University Press, Ithaca).
Furukawa, T., and K. Ishizu, 2005, Macromolecules **38**, 2911.
Gorodyska, G., A. Kiryi, S. Minko, C. Tsitsilianis, and M. Stamm, 2003, Nano Lett. **3**, 365.
Gottwald, D., C. N. Likos, G. Kahl, and H. Löwen, 2004, Phys. Rev. Lett. **92**, 068301.
Gottwald, D., C. N. Likos, G. Kahl, and H. Löwen, 2005, J. Chem. Phys. **122**, 074903.
Grest, G. S., L. J. Fetters, J. S. Huang, and D. Richter, 1996, Adv. Chem. Phys. **XCIV**, 63.
Grimson, M. J., and M. Silbert, 1991, Mol. Phys. **74**, 397.
Groenewegen, W., S. U. Egelhaaf, A. Lapp, and J. R. C. van der Maarel, 2000, Macromolecules **33**, 3283.
Groenewegen, W., A. Lapp, S. U. Egelhaaf, and J. R. C. van der Maarel, 2000, Macromolecules **33**, 4080.
Grosberg, A. Yu., T. T. Nguyen, and B. I. Shklovskii, 2002, Rev. Mod. Phys. **74**, 329.
Hansen, J.-P., and H. Löwen, 2000, Annu. Rev. Phys. Chem. **51**, 209.
Hansen, J.-P., and I. R. McDonald, 2005, *Theory of Simple Liquids*, 3rd ed. (Academic, London).
Hansen, J.-P., and L. Verlet, 1969, Phys. Rev. **184**, 151.
Harreis, H. M., A. A. Konryshev, C. N. Likos, H. Löwen, and G. Suttmann, 2002, Phys. Rev. Lett. **89**, 018303.
Harreis, H. M., C. N. Likos, and H. Löwen, 2003, Biophys. J. **84**, 3607.
Heinrich, M., M. Rawiso, J. G. Zilliox, P. Lessieur, and J. P. Simon, 2001, Eur. Phys. J. E **4**, 131.
Hoffmann, N., C. N. Likos, and H. Löwen, 2004, J. Chem. Phys. **121**, 7009.
Huang, F., K. Addas, A. Ward, N. T. Flynn, E. Velasco, M. F. Hagan, Z. Dogic, and S. Fraden, 2009, Phys. Rev. Lett. **102**, 108302.
Jusufi, A., 2006, J. Chem. Phys. **124**, 044908.
Jusufi, A., C. N. Likos, and M. Ballauff, 2004, Colloid Polym. Sci. **282**, 910.
Jusufi, A., C. N. Likos, and H. Löwen, 2002a, Phys. Rev. Lett. **88**, 018301.
Jusufi, A., C. N. Likos, and H. Löwen, 2002b, J. Chem. Phys. **116**, 11011.
Kapnistos, M., D. Vlassopoulos, G. Fytas, K. Mortensen, G. Fleischer, and J. Roovers, 2000, Phys. Rev. Lett. **85**, 4072.
Kegler, K., M. Konieczny, G. Dominguez-Espinoza, C. Gutsche, M. Salomo, F. Kremer, and C. N. Likos, 2008, Phys.

Rev. Lett. **100**, 118302.
Kegler, K., M. Salomo, and F. Kremer, 2007, Phys. Rev. Lett. **98**, 058304.
Kiryi, A., G. Gorodyska, S. Minko, M. Stamm, and C. Tsitsilianis, 2003, Macromolecules **36**, 8704.
Klein Wolterink, J., F. A. M. Leermakers, G. J. Fleer, L. K. Koopal, E. B. Zhulina, and O. V. Borisov, 1999, Macromolecules **32**, 2365.
Konieczny, M., and C. N. Likos, 2007, Soft Matter **3**, 1130.
Korobko, A. V., W. Jesse, S. U. Egelhaaf, A. Lapp, and J. R. C. van der Maarel, 2004, Phys. Rev. Lett. **93**, 177801.
Korobko, A. V., W. Jesse, A. Lapp, S. U. Egelhaaf, and J. R. C. van der Maarel, 2005, J. Chem. Phys. **122**, 024902.
Kramarenko, E. Yu., A. R. Khokhlov, and K. Yoshikawa, 2000, Macromol. Theory Simul. **9**, 249.
Lang, A., C. N. Likos, M. Watzlawek, and H. Löwen, 2000, J. Phys.: Condens. Matter **12**, 5087, and references therein.
Leermakers, F. A. M., M. Ballauff, and O. V. Borisov, 2008, Langmuir **24**, 10026.
Likos, C. N., 2001, Phys. Rep. **348**, 267.
Likos, C. N., 2006, Soft Matter **2**, 478.
Likos, C. N., R. Blaak, and A. Wynveen, 2008, J. Phys. Condens. Matter **20**, 494221.
Likos, C. N., H. Löwen, M. Watzlawek, B. Abbas, O. Jucknischke, J. Allgaier, and D. Richter, 1998, Phys. Rev. Lett. **80**, 4450.
Louis, A. A., 2002, J. Phys.: Condens. Matter **14**, 9187.
Manning, G. S., 1969, J. Chem. Phys. **51**, 924.
Mei, Y., M. Hoffmann, M. Ballauff, and A. Jusufi, 2008, Phys. Rev. E **77**, 031805.
Mei, Y., K. Lauterbach, M. Hoffmann, O. V. Borisov, M. Ballauff, and A. Jusufi, 2006, Phys. Rev. Lett. **97**, 158301.
Mohanty, P. S., and W. Richtering, 2008, J. Phys. Chem. B **112**, 14692.
Muller, F., M. Delsanti, L. Auvray, J. Yang, Y. J. Chen, J. W. Mays, B. Deme, M. Tirrel, and P. Guenoun, 2000, Eur. Phys. J. E **3**, 45.
Ni, R., D. Cao, W. Wang, and A. Jusufi, 2008, Macromolecules **41**, 5477.
Pincus, P., 1977, Macromolecules **10**, 210.
Pincus, P., 1991, Macromolecules **24**, 2912.
Plamper, F. A., H. Becker, M. Lanzendorfer, M. Patel, A. Wittemann, M. Ballauff, and A. H. E. Müller, 2005, Macromol. Chem. Phys. **206**, 1813.
Plamper, F. A., A. Walther, A. H. E. Müller, and M. Ballauff, 2007, Nano Lett. **7**, 167.
Roger, M., P. Guenoun, F. Muller, L. Belloni, and M. Delsanti, 2002, Eur. Phys. J. E **9**, 313.
Rogers, F. J., and D. A. Young, 1984, Phys. Rev. A **30**, 999.
Rühe, J., M. Ballauff, M. Biesalski, P. Dziezok, F. Gröhn, D. Johannsmann, N. Houbenov, N. Hugenberg, R. Konradi, S. Minko, M. Motornov, R. R. Netz, M. Schmidt, C. Seidel, M. Stamm, T. Stephan, D. Usov, and H. N. Zhang, 2004, Adv. Polym. Sci. **165**, 79.
Santangelo, C. D., and A. W. C. Lau, 2004, Eur. Phys. J. E **13**, 335.
Schneider, C., A. Jusufi, R. Farina, F. Li, P. Pincus, M. Tirrell, and M. Ballauff, 2008, Langmuir **24**, 10612.
Shusharina, N. P., and M. Rubinstein, 2008, Macromolecules **41**, 203.
Stellbrink, J., G. Rother, M. Laurati, R. Lund, L. Willner, and D. Richter, 2004, J. Phys.: Condens. Matter **16**, S3821.
Stillinger, F. H., 1976, J. Chem. Phys. **65**, 3968.
van Roij, R., M. Dijkstra, and J.-P. Hansen, 1999, Phys. Rev. E **59**, 2010.
von Ferber, C., A. Jusufi, M. Watzlawek, C. N. Likos, and H. Löwen, 2000, Eur. Phys. J. E **2**, 311.
Wang, H., and A. R. Denton, 2004, Phys. Rev. E **70**, 041404.
Wang, H., and A. R. Denton, 2005, J. Chem. Phys. **123**, 244901.
Watzlawek, M., C. N. Likos, and H. Löwen, 1999, Phys. Rev. Lett. **82**, 5289.
Watzlawek, M., H. Löwen, and C. N. Likos, 1998, J. Phys.: Condens. Matter **10**, 8189.
Wittemann, A., M. Drechsler, Y. Talmon, and M. Ballauff, 2005, J. Am. Chem. Soc. **127**, 9688.
Witten, T. A., and P. Pincus, 1987, Europhys. Lett. **3**, 315.
Witten, T. A., and P. A. Pincus, 1986, Macromolecules **19**, 2509.
Zhulina, E. B., O. V. Borisov, and T. M. Birshtein, 1999, Macromolecules **32**, 8189.
Zhulina, E. B., O. V. Borisov, V. A. Pryamitsyn, and T. M. Birshtein, 1991, Macromolecules **24**, 140.
Ziherl, P., and R. D. Kamien, 2000, Phys. Rev. Lett. **85**, 3528.
Ziherl, P., and R. D. Kamien, 2001, J. Phys. Chem. B **105**, 10147.